

**METAMORPHIC PETROLOGY AND STRUCTURE OF METAPELITES IN  
THE EASTERN AXIAL ZONE OF THE MONTAGNE NOIRE GNEISS DOME,  
MONTAGNE NOIRE, FRANCE**

**Stephanie J. Moore**

Submitted to the Department of Geology  
Of Smith College in partial fulfillment  
Of the requirements for the degree of  
Bachelor of Arts with Honors

John B. Brady, Faculty Advisor

May, 2006

## Table of Contents

Abstract.....	ii
Acknowledgements.....	iv
List of Figures.....	v
List of Tables.....	vii
INTRODUCTION.....	viii
GEOLOGIC SETTING.....	1
<b>Variscan Belt and the French Massif Central</b> .....	1
<b>Montagne Noire</b> .....	2
<b>Deformation</b> .....	4
<b>Lithologies</b> .....	5
<b>Metamorphic History</b> .....	6
FIELD OBSERVATIONS.....	12
<b>L’Espinouse</b> .....	12
<b>Rosis Syncline</b> .....	18
<b>Le Caroux</b> .....	18
<b>Lineations and Foliations</b> .....	21
PETROGRAPHY.....	24
<b>L’Espinouse</b> .....	24
<b>Rosis Syncline</b> .....	26
<b>Le Caroux</b> .....	30
GEO THERMOBAROMETRY.....	35
MONAZITE DATING.....	47
DISCUSSION.....	56
<b>L’Espinouse</b> .....	56
<b>Rosis Syncline</b> .....	57
<b>Le Caroux</b> .....	59
CONCLUSION.....	68
REFERENCES.....	69
APPENDICES.....	72

## ABSTRACT OF THESIS

### METAMORPHIC PETROLOGY AND STRUCTURE OF METAPELITES IN THE EASTERN AXIAL ZONE OF THE MONTAGNE NOIRE GNEISS DOME, MONTAGNE NOIRE, FRANCE

Stephanie J. Moore  
John B. Brady, Faculty Advisor

The French Massif Central is the south-vergent orogenic wedge of the Southern European Variscides. The Montagne Noire Gneiss Dome comprises the Axial Zone of the Montagne Noire, which is the southernmost extent of the French Massif Central. Extensive studies of the deformational history of the Montagne Noire have been undertaken in recent years, however studies of the metamorphic history have not been as thorough. This study looks at the differences in the metamorphic histories of the various parts of the Montagne Noire Gneiss Dome.

The peak metamorphic grade in L'Espinouse, potentially as low at the biotite-chlorite zone, is lower than the peak grades in the Rosis Syncline and Le Caroux. The metamorphic grades of both the Rosis Syncline and Le Caroux increase from east to west, toward the core of the gneiss dome. Phyllitic rocks in L'Espinouse yielded peak temperatures of  $500 \pm 25$  °C using the biotite-tourmaline thermometer and the abundance of chlorite and the lack of garnet, staurolite, and aluminosilicates suggest that peak metamorphism was in the chlorite-biotite zone. The metamorphic grade increases from east to west, toward the core of the dome, in the Rosis Syncline. Peak temperatures in the metasedimentary envelope reached at least  $575 \pm 50$  °C while metatexites in the core with an assemblage biotite + fibrolite + cordierite(?) are up-grade from the muscovite-out isograd and indicate temperatures over 650 °C. The metamorphic grade also increases from east to west in Le Caroux. Unfortunately, the low-Al bulk composition of these

rocks does not allow for mineral assemblages conducive to tightly constraining the succession of isograds across the subdome. However, the mineral assemblages combined with GTB show a transition from the kyanite zone to the sillimanite zone at the approach of the core. Monozites, enriched in Y from garnet breakdown, yield ages around 310 Ma. These same samples exhibit three distinctly orthogonal cleavages that represent at least two deformation pulses or events. Garnet breakdown in Le Caroux, possibly coincident with a shearing event (gravitational collapse?) in the metasedimentary envelope occurred around 310 Ma as recorded by monazite growth. This shearing event may have postdated a shortening event recorded in a cleavage orthogonal to the shearing cleavage.

Stephanie J. Moore  
Smith College Department of Geology  
Northampton, MA 01063  
May, 2006

## ACKNOWLEDGEMENTS

John Brady has been the best possible advisor I can imagine. He supported and encouraged me each step of the way, but most importantly he gave me the space to work independently. When I did go to him with questions, the long and winding answers (with many digressions) were always the best because they fueled me with more questions and ideas. Last year John asked me an important question about my confidence. I will be forever grateful to him for showing me how important it is for me to believe in my abilities as a scientist and to take pride in my work.

I would like to thank all of the professors in the Smith College geology department for their incredible dedication to teaching and their contagious passion for geology. Ann Pufall I thank for her wise words and Kathy Richardson for her warm smiles and help with all the paperwork. Tony Caldanaro provided much needed comic relief and also keeps the best rock room and thin section lab that I have had the pleasure of using! Richard Briggs and Judith Wopereis worked their magic with the SEM and I thank them for their patience.

I would like to thank professors Christian Teyssier and Donna Whitney at the University of Minnesota for helping me design this project and for providing me with the opportunity to combine my interests in structural geology and metamorphic petrology. Donna contributed many helpful comments and suggestions regarding the geothermobarometry work and extended an invitation to ask any questions I had along the way.

Professors Michael Jercinovic and Michael Williams at the University of Massachusetts at Amherst were an incredible resource for the monazite dating; I thank them for all of the time they spent processing my samples and discussing the results with me.

Jenny Haywood was an enthusiastic field assistant and I thank her for her endless supply of conversation, knowledge of gneiss domes, and Nutella. Sarah Hale and Kelsey Winsor were great cavemates this year and I could not have pushed through the more difficult times without them.

I would like to thank all of my friends and family for their support in my academic endeavors. I especially thank Gary Peckman for giving me the freedom to choose Smith and for encouraging me to do what I love.

## LIST OF FIGURES

Figure	Page Number
1. Map of the Montagne Noire after Roger (2004).....	3
2. Geologic map of the eastern end of the Axial Zone..... with isograds after Thompson and Bard (1982)	7
3. Sample location map.....	13
4. Field photo of shear band at station 19.....	14
5. Photomicrograph of sample 33 from L’Espinouse.....	15
6. Field photo of sigma clasts at station 16.....	17
7. Field photo of isoclinal folds at station 13.....	20
8. Stereoplots of foliations.....	22
9. Stereoplot of lineations.....	23
10. Backscattered electron images of carbonates in sample 15.....	27
11. CFM diagram for sample 15 carbonates.....	28
12. Photomicrograph of sigma clast in sample 38.....	29
13. Photomicrograph of staurolite porphyroblast.....	31
14. Photomicrograph of sample 03 cleavages.....	32
15. Photomicrograph of sample 13 cleavages.....	34
16. P-T diagrams for samples 01, 02, 03, and 12 from GTB.....	37
17. Petrogenetic grid modified after Spear and Cheney (2000) .....	38
18. P-T diagrams for sample 13 from GTB.....	39
19. P-T diagram for samples 27 and 32 from L’Espinouse from GTB.....	41
20. P-T diagram for sample 03 from TWQ.....	42
21. P-T diagram for sample 02a from TWQ.....	43
22. P-T diagram for sample 01b from TWQ.....	44
23. Element maps for garnet from sample 03.....	45
24. Monazite analysis locations for sample 13.....	48
25. Element maps for monazites from sample 13.....	50
26. Age histogram for sample 13.....	51
27. Monazite analysis locations for sample 03.....	52
28. Element maps for monazites from sample 03.....	53

29. Age histogram for sample 03.....	55
30. Sample location map with MUS isograd.....	58
31. AFM diagram with 02a bulk composition.....	60
32. P-T diagram for samples 01, 02, 03, and 13.....	62

LIST OF TABLES

Table	Page Number
1. Mineral assemblages.....	25



## INTRODUCTION

The Montagne Noire Gneiss Dome is located in the Axial Zone of the Montagne Noire mountains in the southeastern French Massif Central and formed during the Variscan continental collision of Gondwana and Laurasia (Aerden and Malavieille, 1999). Within the gneiss dome are two subdomes, L'Espinouse to the north and Le Caroux to the south. A gneiss dome is a structure that comprises high-grade metamorphic rocks or plutonic rocks showing a concentric and outward-dipping gneissic foliation (Yin, 2004; Whitney et al., 2004). Generally, high-grade schists and gneisses cover a core of migmatites (Whitney et al., 2004).

Much debate over the structural evolution of the Montagne Noire Gneiss Dome has been carried out over the last fifteen years (e.g. Aerden and Malavieille, 1999; Aerden, 1998; Echtler, 1990), but little attention has been paid to the difference in the metamorphic petrology that accompanies these deformation events in the two subdomes (e.g. Soula et al., 2001). The exposure of rocks in the Montagne Noire Gneiss Dome displays a core of anatectic granites, migmatites, and high-grade metamorphic gneisses mantled by a metasedimentary cover of porphyroblastic schist, metagraywacke, quartzite, minor amphibolite, and calc-silicate rocks (Thompson and Bard, 1982; Van den Driessche and Brun, 1992). Observations from fieldwork and hand specimens indicate that the metasedimentary cover of Le Caroux subdome underwent a higher grade of metamorphism than the metasedimentary cover of L'Espinouse subdome. This study examines both the structural geology and metamorphic petrology of the metasediments in the eastern Montagne Noire to better quantify the different metamorphic histories of L'Espinouse and Le Caroux subdomes.

## GEOLOGIC SETTING

### **Variscan Belt and the French Massif Central**

The Variscan Belt is a mountain chain that stretched 3000 km in length from the Caucasus (Europe) to the southern Appalachian Mountains (North America) before the opening of the Atlantic Ocean (Matte, 2001). The Variscan formed during the Devonian and Carboniferous periods when Gondwana, from the south, collided with Baltica-Laurentia, from the north (Aerden, 1998; Matte, 2001 and references within; Matte, 1986). Smaller micro-plates, mainly Avalonia and Armorica, separated, drifted, and collided between these main plates during the early Paleozoic. As a result of these collisions, deformation, metamorphism and granitic magmatism of the French Massif Central underwent a southward migration during the Devono-Carboniferous period (Echtler and Malavieille, 1990).

Matte (2006) succinctly summarizes the main events in the history of the Variscan. At 450 Ma, a small part of the Galicia-South-Brittany-French Massif Central ocean closed by subduction to the northwest. Then, at 420 Ma Gondwana's passive continental margin and overlying accretionary prism were subducted and underwent high pressure and ultra-high pressure metamorphism. During the Lower to Middle Devonian period, buoyancy caused the thinned continental slice, subducted sediments, and parts of ocean crust and mantle to rise. Northward subduction of the continental crust continued and was followed by southward thrusting and further exhumation of the Leptynitic-Amphibolitic Group by northeastward detachments. In the Upper Devonian and Lower Carboniferous, exhumation was completed and followed by erosion of the Leptynitic-Amphibolitic Group rocks, rifting, calc-alkaline volcanism, and deposition of a marine

series in the northeast French Massif Central. Finally, in the Lower Carboniferous (340-330 Ma) the Brévennes-Morvan series was strongly folded and an unconformable Late-Visean volcanics and coal-bearing series was deposited. At about the same time (Namurian, 320-315 Ma) southward thrusting emplaced the Montagne Noire fold nappes.

### **Montagne Noire**

The French Massif Central (Figure 1) is the south-vergent orogenic wedge of the Southern European Variscides (Soula et al., 2001) and is part of the Ibero-Armorican arc (Matte, 2006). High temperature and low-to-medium pressure metamorphic rocks that have been overridden by ultra-high pressure granulites and eclogites characterize the French Massif Central. The granulites and eclogites have been interpreted as remnants of subducted continental crust with attached oceanic crust slices. Within the French Massif Central, the Montagne Noire is the most external ridge and lies adjacent to the southern Visean foreland basin (Soula et al., 2001).

The Montagne Noire can be divided into three main units: the Northern Flank, the Axial Zone, and the Southern Flank (Figure 1). The Axial Zone comprises the Montagne Noire Gneiss Dome, which is divided into two subdomes. L'Espinouse subdome, to the north, is separated from Le Caroux subdome, to the south, by the Rosis Syncline, a tight, non-cylindrical syncline of metasediments (Van den Driessche and Brun, 1992). A gneiss dome is a structure that comprises high-grade metamorphic or plutonic rocks showing a concentric and outward-dipping gneissic foliation (Yin, 2004 and Whitney et al., 2004). Generally, high-grade schists and gneisses cover a core of gneissic rocks like migmatites or orthogneisses (Whitney et al., 2004). The exposure of rocks in the

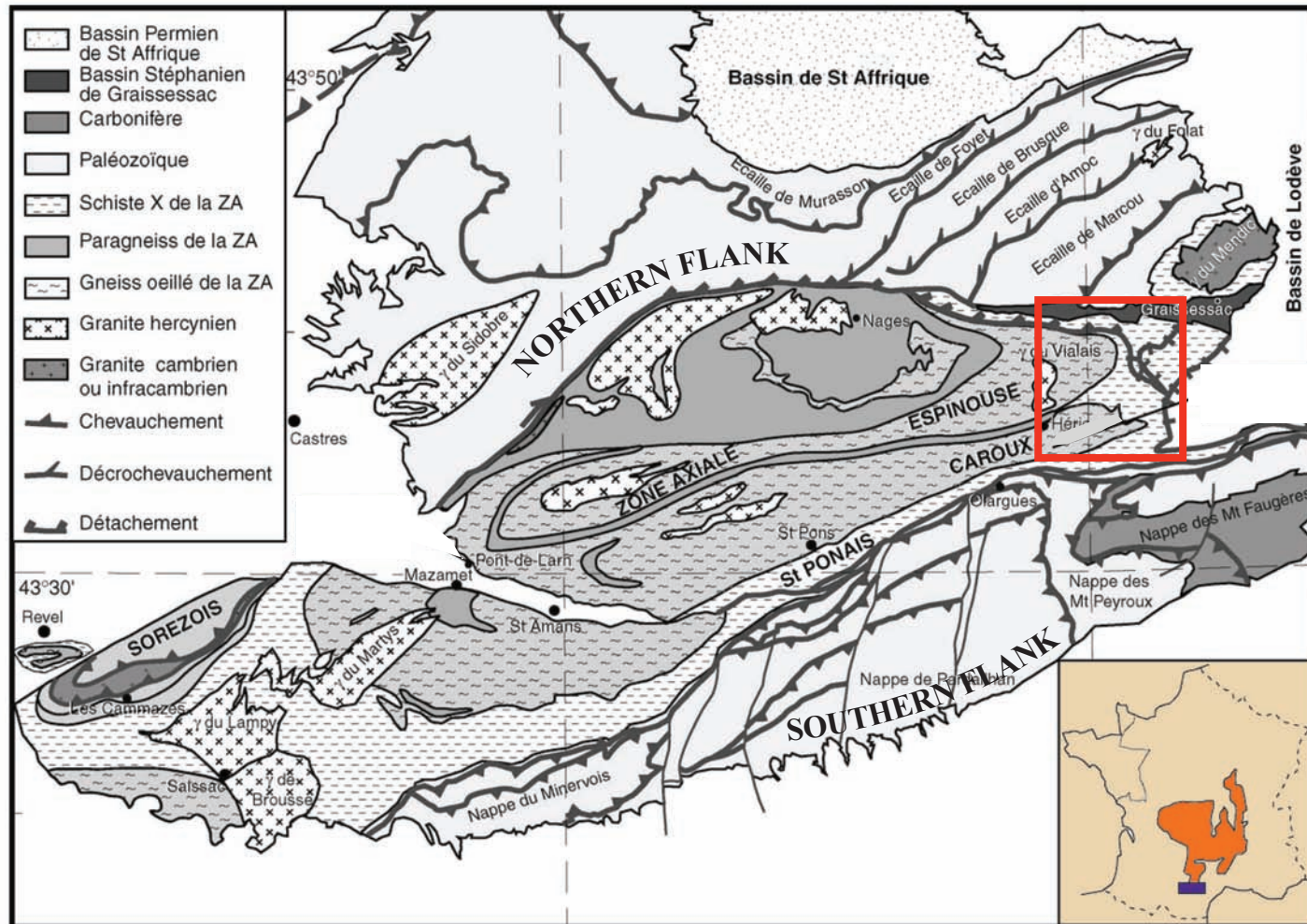


Figure 1. Map of the Montagne Noire with the study area outlined in red. In the inset France is tan, the Massif Central is orange, and the Montagne Noire is purple (modified after Roger, 2004).

Montagne Noire Gneiss Dome displays a core of metamorphic gneisses, migmatites, and anatectic granites mantled by a metasedimentary cover of porphyroblastic schists, metagraywackes, quartzites, minor amphibolites, and calc-silicates (Thompson and Bard, 1982; Van den Driessche and Brun, 1992).

### **Deformation**

The explanation of the deformation history of the Montagne Noire has undergone significant revision in the literature since Bard and Rambeloson (1973) first described a series of schistositys ( $S_1$ ,  $S_2$ ,  $S_3$ ), in which  $S_1$  and  $S_2$  were characterized by isoclinal folding. Wierderer et al. (2002) have compressed the description of the deformation history into three periods of deformation: D1 was a period of high pressure and crustal thickening when Paleozoic sediments deformed into large recumbent fold nappes stacked by southward thrusting; D2 encompasses the extension and exhumation of the Axial Zone and left a record of low pressure and high temperature metamorphism; and D3 was a period in which the refolding of the Southern Flank created map scale antiforms and synforms. This three-event deformation history has been expanded and modified and most researchers agree that the Montagne Noire experienced five major microstructural events. D1 and D2 correspond to early thrusting; D3 to steep folding; D4 to detachment tectonics with coaxial strain, extension parallel to the long axis of the dome, and vertical shortening and longitudinal stretching; and D5 to wrench tectonics (Aerden, 1998; Soula et al., 2001).

Several differences in the deformational histories of Le Caroux and Espinouse have been cited in recent literature. “Significant differences in strain pattern suggest a

diachronism of deformation within Le Caroux and L'Espinouse domes respectively” (Van den Driessche and Brun, 1992). Shear bands are found in both Le Caroux dome and L'Espinouse dome. Only C' type shear bands have been identified in Le Caroux dome, while C' and C type shear bands have been located in L'Espinouse dome. Also found in L'Espinouse is a 30 – 60 m thick C/S mylonite along the northern border and eastern closure of the dome. The presence of C/S structures is characteristic of retrograde deformation histories. Strike lines of foliation and shear planes are oblique to each other in L'Espinouse, while in Le Caroux the foliation planes between adjacent shear bands are folded. This folding indicates “initial obliquity between the foliation and shear bands direction” and suggests two stages of deformation in Le Caroux. “Foliation and shear bands in L'Espinouse dome are coeval and strain pattern analysis does not show any evidence of preserved fabrics related to an older deformation in contrast to the deformation in Le Caroux dome” (Van den Driessche and Brun, 1992).

### **Lithologies**

The Montagne Noire stratigraphic pile consists of Neoproterozoic and Paleozoic rocks. The Paleozoic rocks were originally a thick series of shales interbedded with volcanics and carbonates. During the early and middle Paleozoic, crustal and lithospheric thinning led to sedimentation in an extensional basin in the northern Montagne Noire while at this time the southern region was covered with shallow-marine deposits (Soula et al., 2001 references within). Dating on single zircons of metadacite interlayers yield ages of  $545 \pm 15$  Ma (Lescuyer and Cocherie, 1992) for the uppermost part of the series; dating of the lower, intruded granitic sheets yield ages of  $513 \pm 13$  Ma (Ducrot et al., 1979).

Previous workers have divided exposures of rocks in the Montagne Noire into three regions: the Northern Units, the Axial Zone, and the Southern Units. The Northern Flank is a greenschist facies Lower Paleozoic series of south-eastward-vergent thrust sheets (Soula et al., 2001). The Axial Zone is an ENE-WSW trending elongate dome. A steeply-dipping fault separates L'Espinouse and Le Caroux subdomes. The core of the dome is Proterozoic to early Paleozoic (Echtler and Malavieille, 1990) migmatized orthogneiss locally intruded by either late-Hercynian granodiorites (Soula et al., 2001) or late-Hercynian anatectic gneisses (Echtler and Malavieille, 1990). The core of L'Espinouse has metasedimentary septa of metapelites, metaquartzites, marbles and metabasites. The envelope surrounding the core on the eastern end, better known as the Schistes-X, is primarily late Proterozoic to Early Cambrian (Echtler and Malavieille, 1990) micaschists, carbonates, and calcium-magnesium rich rocks (Bard and Rambeloson, 1973). The Southern Units are low-grade to non-metamorphic thrust sheets of Cambrian to Lower Carboniferous terrains involved in stacking into the Viséan foreland basin (Soula et al., 2001). This paper focuses on the metasedimentary envelope of the eastern end of the Axial Zone.

### **Metamorphic History**

Thompson and Bard (1982) performed a detailed transect across the Rosis Syncline through the metasedimentary envelope and published isograds that, from east to west, are marked by the first appearance of biotite, cordierite, staurolite, and sillimanite (Figure 2). The closely spaced isograds dip gently eastward. They wrap tightly around L'Espinouse but diverge southward due to topographic relief. To the north of L'Espinouse the

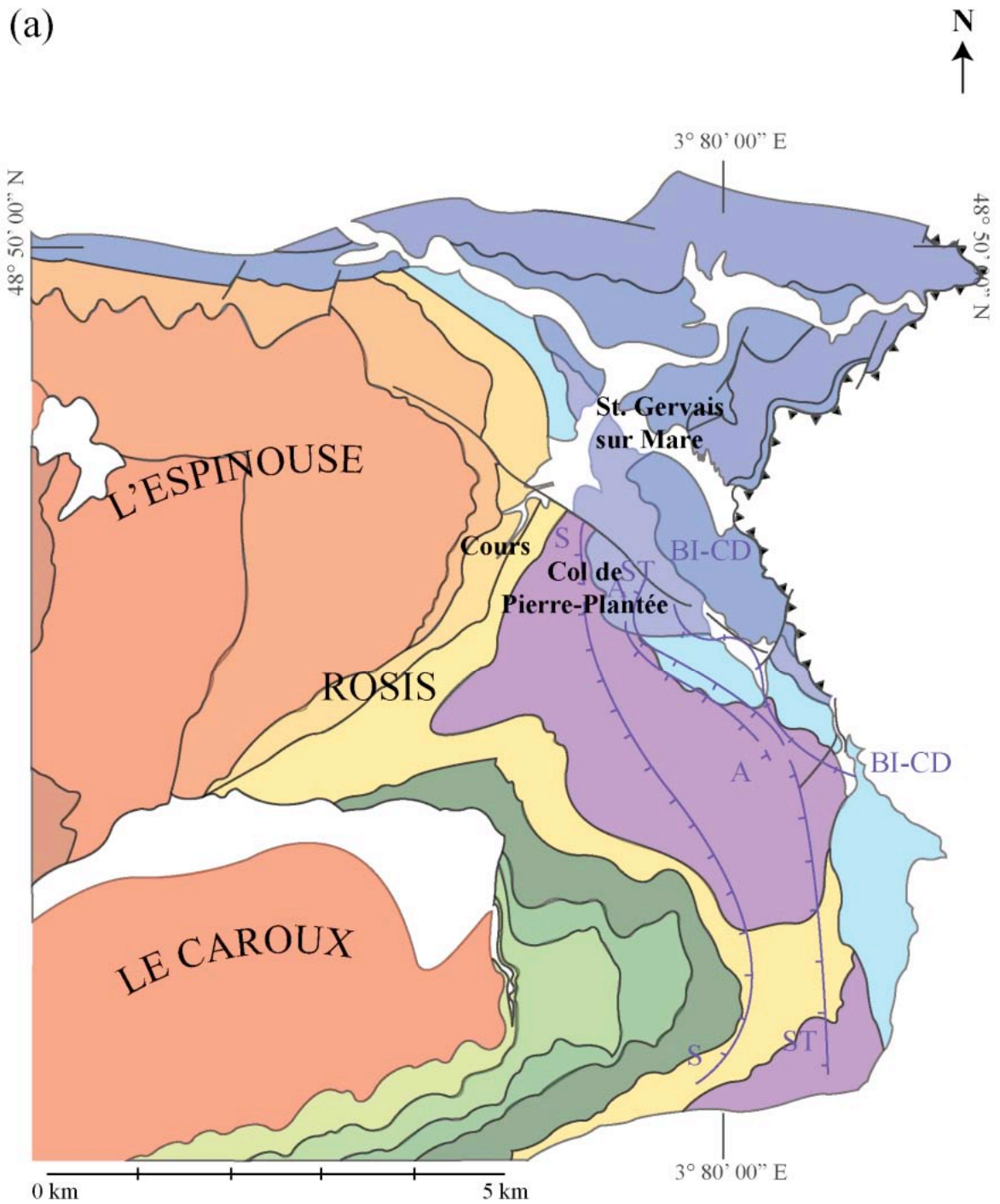
















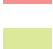





Figure 2. (a) Geologic map of the eastern end of the Zone Axiale in the Montagne Noire Gneiss Dome, Montagne Noire, France with isograds after Thompson and Bard (1982). Mineral abbreviations: BI = biotite, CD = cordierite, ST = staurolite, A = andalusite, and S = sillimanite. Station locations are plotted and numbered. (b) Legend.



(b)

-  Isograds with hatchmarks denoting upgrade direction
-  Observed contact
-  Fault
-  Thrust fault
  
-  Cover
-  X11 Siliceous schists and schists subardoisiers has beds tuffaces
-  X10 St. Gervais schist
-  X9 Barry schist
-  X8 Lamalou Metacerinite
-  X7 Senas-Le-Cros micaschist
-  X6 Col de Madale micaschist
-  X5 Torteillan micaschist
-  X4 Combes gneiss
-  X3 Vernet gneiss
-  X3-5 Fine-grained gneisses with biotite
-  L: Gneiss and migmatite
-  pL Gneiss oeilles has planar foliation
-  mL Leucocratic gneiss with fine foliation
-  L-lambda
-  Gamma: Homogeneous granite (cordierite)

isograds are cross-cut by low-angle normal faulting leaving the low-grade rocks of the Lacaune Mountains Thrusts and Stephanian sediments of the Graissessac basin juxtaposed against high-grade gneisses in the dome (Van den Driessche and Brun, 1992). The isograds in Le Caroux display a similar pattern but show no metamorphic discontinuity (Van den Driessche and Brun, 1992). According to Echtler and Malavieille (1990), “The abnormally tight metamorphic succession, telescoping in about 1 km high-grade sillimanite-rich gneisses with very low grade metamorphosed sediments, can be related to the subtractive effects of the synmetamorphic tectonic denudation.” Prograde metamorphism progressed from the schist to the migmatites with a discontinuity at the contact between the schist and the migmatites. A 150-200 m thick transition zone of alternating orthogneissic and metasedimentary sheets several meters thick is strongly deformed and displays mylonitic foliation parallel to the contact. These are indications of gneissic uplift relative to the envelope. Higher and/or faster uplift of the core relative to the envelope causing high temperature decompression is one explanation for the discontinuity in L’Espinouse (Soula et al., 2001).

Although the explanations for the metamorphism are controversial, there is a consensus in the literature that the Hercynian metamorphism of the Montagne Noire was high temperature and low pressure (HT-LP). Two stages of metamorphism have been defined in the envelope. Soula et al. (2001) summarize the two stages:

“Stage 1 metamorphism was prograde with the succession of biotite, staurolite, kyanite, and prismatic sillimanite zones. Stage 2 metamorphism is represented by well-defined isograds with the succession of biotite II, cordierite, andalusite, and fibrolitic sillimanite zones. Stage 1 and Stage 2 minerals are all aligned with S1

and the succession of the mineral assemblages is interpreted here as a continuous process occurring during progressing strain.”

Peak metamorphic conditions of 620 °C and 4.5 kbar at the contact between the metasedimentary schists and the gneissic core occurred in stage 1; Stage 2 saw an increase in temperature and a decrease in pressure as seen in the transformation from staurolite into cordierite and staurolite into andalusite . This suggests a clockwise P-T-t path that also explains the evolution of the core of the Montagne Noire. The gneissic core also saw peak metamorphic conditions during Stage 1 of the metamorphic history (Soula et al., 2001). But the core was hotter and deeper than the envelope reaching temperatures of 700°C (Ourzik et al., 1991) and pressures of  $5 \pm 0.5$  kb (Ourzik, 1993). Stage 2 saw lower pressures and temperatures of 650°C at 3kb (Ourzik et al., 1991) and pressures and temperatures continued to drop to 600°C and 2.5 kbar during stage 3 (Ourzik, 1993).

There is a debate among researchers over the cause of the HT-LP Carboniferous metamorphism. The dominant hypothesis is that the metamorphism was caused by the Hercynian orogeny and accompanied by the intrusion of late Carboniferous granites (Cocherie et al., 2005). Wiederer et al. (2002) rule out regional metamorphism as the main mechanism for HT-LP metamorphism in the Montagne Noire Gneiss Dome. Their line of reasoning is as follows: Isotopic studies (Franke et al., 2002) record HT/LP metamorphism in the gneisses active at  $316 \pm 1$  Ma or after the intrusion of the post-tectonic Vialais granite at  $327 \pm 5$  Ma (Matte et al., 1998). Because flysch sedimentation continued into 325-320 Ma (Menning et al., 2000) there was not enough time for a regional metamorphism caused by stacking and followed by thermal relaxation. They

conclude that dynamic contact metamorphism was at work. Aerden (1998) presents the following age constraints for the metamorphism of the Montagne Noire. The eclogites in the southern Montagne Noire have an Eo-Variscan origin between 380 Ma and 340 Ma and are prior to D2. Steep folding (D2) is post 340 Ma. There is a long history of granitic intrusions spanning multiple deformational events between 340 and 280 Ma with peaks at 330 Ma (synorogenic) and 290 Ma (postorogenic). Peak metamorphic conditions were around 600°C at 325 Ma and 375°C (closing temperature of muscovite) at 300 Ma. And finally, wrench tectonics are post 295 Ma.

Based on mineral assemblages from the core of the metatexites in the migmatitic part of the Laouzas massif (granite massif in the Axial Zone of L'Espinouse), L'Espinouse underwent a clockwise PT-t curve. Melting of sediments followed by segregation of anatectic magma and crystallization resulted in the spacial displacement of anatectic magmas from about 15 km up to their final emplacement at about 5 to 6 km (Ourzik et al., 1991)

## FIELD OBSERVATIONS

Thirty-eight locations in the Montagne Noire Gneiss Dome were investigated and are plotted on the sample map of the region in Figure 3.

### **L'Espinouse**

#### *North of St. Gervais sur Mare*

The rocks north of St. Gervais sur Mare are phyllites and calc-silicates with grain sizes so small that it was not possible to distinguish individual grains in the field. The phyllites at station 19 are folded at the outcrop scale. Another example of deformation is the 3 cm-thick shear band pictured in Figure 4 with top-to-the-east sense of shear. Samples from station 20 are calc-silicates. Similar folds at this outcrop range from 3 cm to 1 m in width and indicate ductile deformation. Because of the extreme weathering and similarity to station 19 no samples were collected. Except for the quartz boudins/ribbons that stretch NE/SW, the siliceous phyllite from station 21 looks very similar to the phyllites from stations 19 and 20.

Samples from stations 33 and 34 are phyllites (Figure 5) that are mapped as meta-dolerites from unit X<sub>10</sub>. Phyllites at station 33 have been folded at a scale of 1 cm to 1 m. Samples from station 35 in unit X<sub>8</sub> are crenulated schist interbedded with layers of a very fine-grained chalky rock. These layers are up to 1 cm thick and may be what is referred to in unit X<sub>8</sub> as the meta-cinerite (incinerate?).

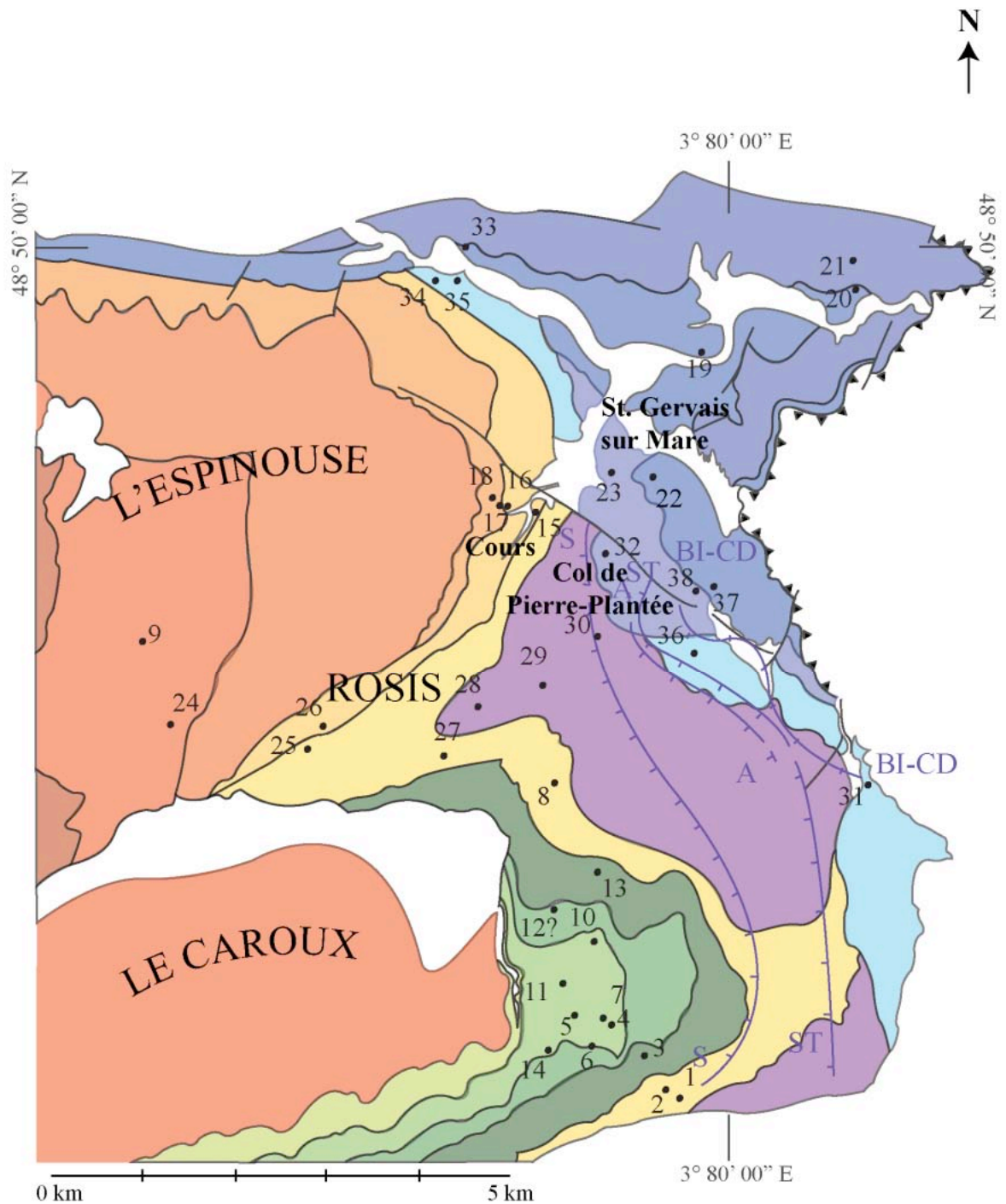


Figure 3. Sample location map from the eastern end of the Zone Axiale in the Montagne Noire Gneiss Dome, Montagne Noire, France with isograds after Thompson and Bard (1982). Mineral abbreviations: BI = biotite, CD = cordierite, ST = staurolite, A = andalusite, and S = sillimanite. Station locations are plotted and numbered.

W

E



Figure 4. A shear band at station 19 indicates a top-to-the-east sense of shear. 15 cm pencil for scale.



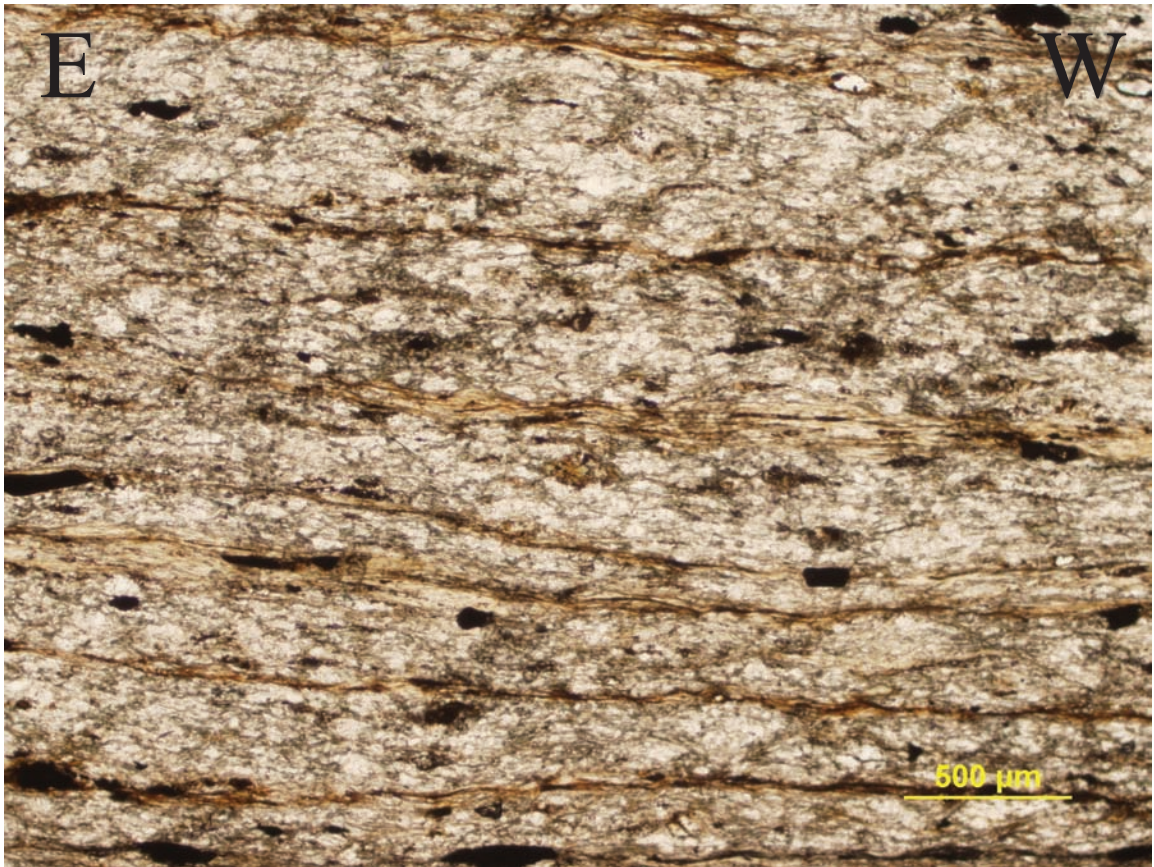


Figure 5. Photomicrograph of sample 33 from L'Espinouse.



### *Cour*

The samples from Cour represent a traverse from the Cour parking lot, which resides in the structurally higher units  $X_{3-5}$ , to the structurally lower unit  $m\zeta$ . This is also the transition from the mantling schists to the beginning of the migmatitic core of the gneiss dome. The dolomitic? calc-silicate from station 15 in the Cour parking lot is folded at the millimeter to centimeter-scale. This rock is an example of the more calcareous rocks that are found with the pelitic phyllites in L'Espinouse. Feldspar porphyroblasts in the rock at station 16 indicate a top-to-the-northeast sense of shear (Figure 6). Sample 18 is a schisty-gneiss in unit  $m\zeta$  with feldspar porphyroclasts up to 5 cm across. No samples were collected farther into the core of the dome, but the rocks are much more migmatitic and evidence of partial melting is abundant.

### *Col de Pierre Plantée*

I have classified the samples from the Col de Pierre Plantée as phyllites. The rocks at station 22 are very similar to those seen at stations 19 and 20 to the northeast in L'Espinouse. These calc-silicates have large-scale folds and distinct layering. Except for stations 37 and 38 where no folds were visible, all of the other stations in the Col de Pierre Plantée exhibit folds on the scale of several centimeters across the limbs (station 30) up to several meters (station 32 and 22). Clasts/veins of quartz up to 1 cm in width were found in the fine-grained dark matrix from the hand samples from station 37.

W

E



Figure 6. Feldspar sigma clasts indicate a top-to-the east sense of shear in the augen gneiss from station 16 along the Cour transverse. Pencil for scale. Black part of pencil is 1.5 cm.

## **Rosis Syncline**

The ENE plunging Rosis Syncline divides L'Espinouse and Le Caroux subdomes in the mantling schists. Station 29 is farthest from the deepest part of the dome and lies in the X<sub>7</sub> unit. This schist has two generations of folds. One generation of the folds plunges 28° to the east. Station 28 is also in the X<sub>7</sub> unit and the rock type is a sillimanite-schist that is folded at the outcrop scale. Sample 27 is the last example, heading eastward, of a schist with the presence of muscovite, while the rocks at Station 25 are higher-grade, muscovite-free schist. Both of these stations are from unit X<sub>6</sub>. A stream divides station 26; on the stratigraphic up-section side is schist and on the down-section side is fairly massive leucocratic biotite gneiss. This may be the contact between the core of the dome and the metasedimentary envelope. No samples were collected because no fresh surfaces could be located. Station 24 is out of unit m $\zeta$  and in unit  $\zeta$ , which is mapped as a migmatitic gneiss. Discontinuous bands of quartz and feldspar and the presence of leucosomes led me to classify this as a diatexite. At station 24 the grain size ranges from 1 mm to 2 cm in diameter. Station 09 is farther to the north; in the field I was unable to decide whether this was a metatexite or a diatexite, but based on its relationship to station 24, it seems plausible that it is also a diatexite. Slickensides in a shear band indicate that the last increments of frictional sliding were NNE (Van der Pluijm and Marshak, 2004).

## **Le Caroux**

Samples from ten stations were collected from Le Caroux. All samples were collected to the west and above the sillimanite isograd, as defined by Thompson and Bard (1982).

With the exception of sample 06MN01c, which is a calc-silicate, samples from Le

Caroux fall into three categories: coarse to fine-grained schists, fine-grained quartzo-feldspathic gneisses, and grano-diorite orthogneisses.

Samples from stations 01 and 02 come from unit X<sub>6</sub>, the schist unit farthest from the deepest part of the subdome. These garnet-micaschists have strong foliations and stretching lineations defined by biotite. A calc-silicate (dolomite) was also collected from station 01. Similar folds at both outcrops are evidence of ductile deformation.

Samples 03 and 13 were collected from the X<sub>5</sub> unit and are garnet-staurolite schists. The schists at station 13 are isoclinally folded on the scale of centimeters (Figure 7). Station 03 is almost directly south of station 13 on the southeastern most end of Le Caroux subdome. The 150-degree difference between the strikes of the foliations from stations 03 and 13 (083° and 304°, respectively) is in agreement with the antiformal structure of Le Caroux. Station 12 lies on the border between units X<sub>5</sub> and X<sub>4</sub>. Although no centimeter- or meter-scale folds were seen at the outcrop, this schist is crenulated at the millimeter scale.

Sample 07b is the lone schist collected from unit X<sub>3</sub>. The remainders of the samples from Le Caroux are fine-grained quartzo-feldspathic gneisses and augen gneisses. Samples 04, 06, and 11 are fine-grained quartzo-feldspathic gneisses. Distinct foliation planes and a strong stretching lineation defined by biotite are visible at the outcrop-scale at station 11. Although the outcrop is highly weathered, plagioclase porphyroblasts, as large as 1 cm in diameter, indicate a top-to-the-southwest sense of shear.

Augen-gneisses were found at stations 07 and 10. Sigma-clasts from both locations are 2 millimeters in diameter and indicate top-to-the northeast sense of shear.



Figure 7. Photograph of isoclinal folds from station 13. 15 cm pencil for scale.

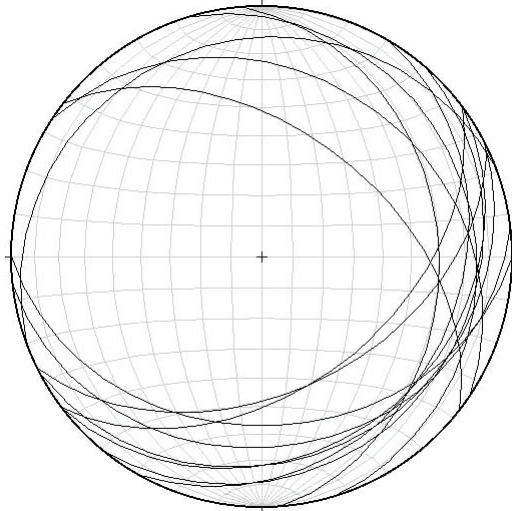
Several delta-clasts from sample station 07 are also in agreement with this shear sense.

Overall, the samples from the stations farthest to the west and closest to the deepest part of the dome displayed the most weathering. The very fine-grained and crenulated white-mica schist from station 14 was so weathered that it was not sampled. Lineations throughout the eastern end of the Montaigne Noire Gneiss Dome are consistently ENE to E. This is aligned with the long axis of the gneiss dome.

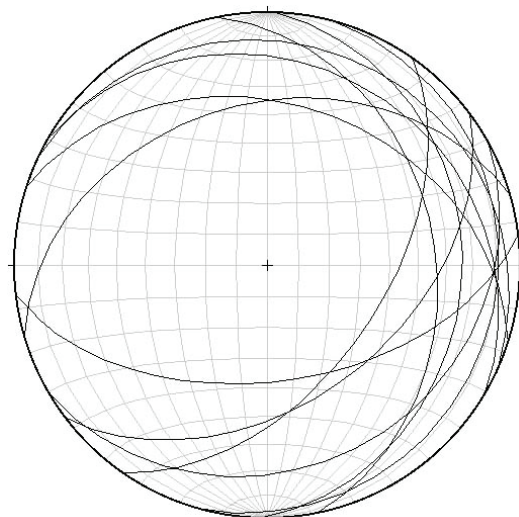
### **Lineations and Foliations**

Foliations from Le Caroux, L'Espinouse, and the Rosis Syncline are plotted in Figure X. The variations in foliation are the result of extensive folding. The strong mineral stretching lineations across the eastern end of the gneiss dome are consistently ENE (Figures 8 and 9). A possible explanation is that the strong stretching lineations are the result of a non-coaxial (rotational) component of strain and the development of a foliation during crustal flow (Vanderhaeghe, 2004). Structural data were plotted using the program Stereonet 6.33 (Allmendinger, R.W., 2002). The foliation orientations show that, although isoclinal folds were found at individual outcrops, the dome, as a whole, was not isoclinally folded.

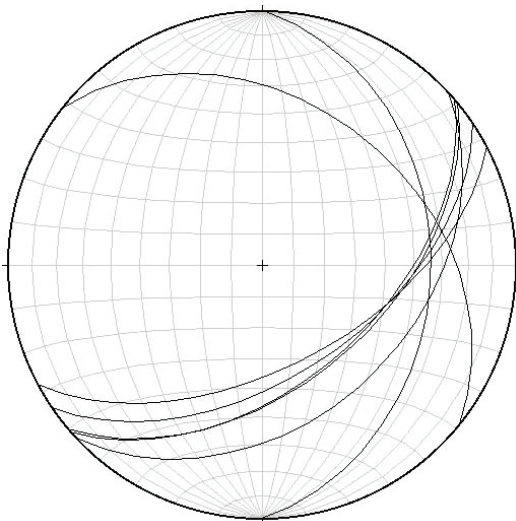




Le Caroux foliations



L'Espinouse foliations



Rosis foliations

Figure 8. Stereoplots of foliations from Le Caroux, L'Espinouse, and the Rosis Syncline. The variations in foliation are the result of extensive folding that generally plunges northeast or southeast in the eastern end of the Montagne Noire.

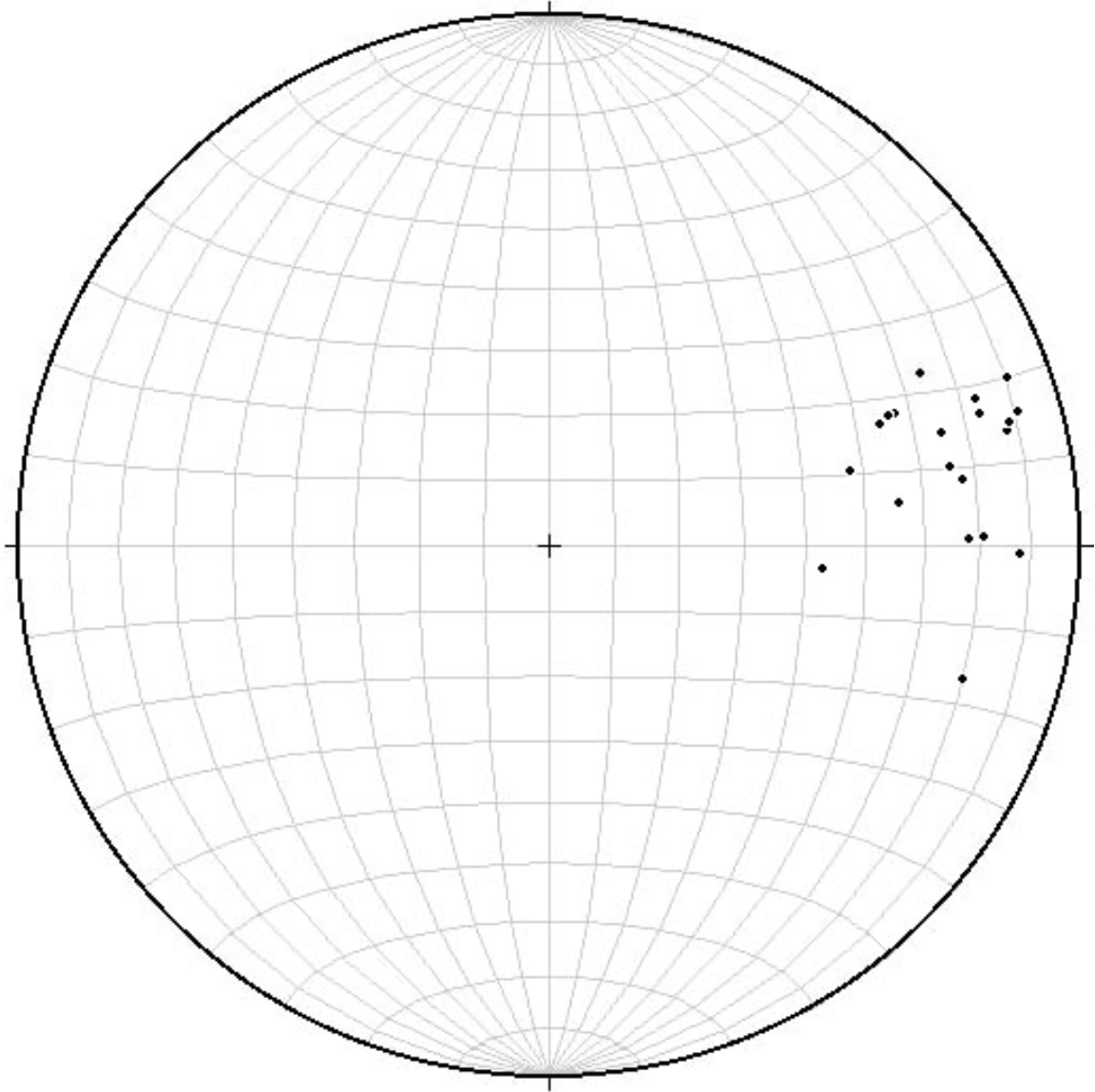


Figure 9. Stereoplot of lineations from the eastern end of the Axial Zone in the Montagne Noire Gneiss Dome. The strong mineral stretching lineations across the eastern end of the gneiss dome are consistently ENE.



## PETROGRAPHY

### **L'Espinouse**

#### *North of St. Gervais sur Mare*

Thin sections were made from four samples that were collected from the areas northeast and northwest of St. Gervais sur Mare in L'Espinouse (Figure 3). Table 1 shows the mineral assemblages of the collected samples. The two samples from the northwest are very fine-grained phyllites with foliation layers less than 50  $\mu$  thick. Individual grains of mica are indistinguishable. Quartz grains in both samples are as large as 250  $\mu$ m, but most are less than 50  $\mu$ m. Sample 06MN21A has a consistently NW/SE stage 3 sigmoidal crenulation cleavage across the sample. The two samples from the northeast are fine-grained schist and phyllite with quartz grains between 50 and 200  $\mu$ m. Sample 06MN33 has distinctive quartz layers separated from micaceous layers signifying a stage 5 crenulation cleavage. It also contains outlines of porphyroblasts of an unknown mineral recrystallized with quartz grains. XRD analysis of sample 33 shows peaks congruent with clinoclhorite. Sample 06MN35 is very weathered with sigmoidal crenulations varying in stage and direction across the thin section.

#### *Cours*

Sample collection from the Cours area (Figure 3 and Table 1) followed a short transect from the metasedimentary envelope into the gneissic core of L'Espinouse. Samples 06MN15a and 06MN15b were from an outcrop in the parking lot near Cours and are very similar, although 06MN15b is more weathered and contains biotite. Sample 15a is a calc-silicate composed of the following minerals: carbonates, quartz, albite, and orthoclase with less than 1% each of barite, rutile chlorite, apatite,

Sample Number	QZ	PL	MUS	CHL	BT	GT	ST	SIL	CA	OP	TO	EP	CZ
<b>L'Espinouse</b>													
<i>North of St. Gervais sur Mare</i>													
06MN19	X	-	X	-	X	-	-	-	-	-	-	-	-
06MN21	X	-	X	-	-	-	-	-	-	O	T	-	-
06MN33	X	-	?	X	?	-	-	?	-	O	T	-	-
06MN35	X	0	X	-	X	-	-	?	-	-	-	-	-
<i>Cours</i>													
06MN16	X	O	O	X	O	-	-	-	-	-	T	-	-
06MN18	?	?	-	?	X	-	-	-	-	-	-	-	-
<i>Col de Pierre Plantée</i>													
06MN22	?	-	?	?	?	-	-	-	-	-	-	-	-
06MN23	X	-	-	-	-	-	-	-	-	-	-	-	-
06MN30	X	O	O	-	X	-	-	-	-	-	T	-	-
06MN32	X	O	-	-	X	-	-	-	-	O	T	-	-
06MN36	X	-	-	-	X	-	-	-	-	-	T	-	-
06MN37	X	-	?	-	?	-	-	?	-	-	T	-	-
06MN38	?	?	?	-	?	-	-	-	-	-	T	-	-
<b>Rosis Syncline</b>													
06MN09	X	O	-	-	O	-	-	O	-	-	-	-	-
06MN25	X	-	-	-	X	-	-	-	-	-	T	-	-
06MN27	X	-	X	-	X	-	-	-	-	-	O	-	-
06MN28	X	-	O	-	O	-	-	O	-	-	O	-	-
06MN29	X	-	X	-	X	-	-	-	-	-	-	-	-
<b>Le Caroux</b>													
06MN01b	X	O	-	-	X	O	-	-	-	O	-	-	-
06MN01c	X	-	-	-	X	-	-	-	-	O	-	X	X
06MN02a	X	O	X	-	X	O	O	?	-	-	T	-	-
06MN02b	X	X	X	-	X	O	O	-	-	-	-	-	-
06MN03	X	O	X	-	X	O	O	-	-	-	-	-	-
06MN05	X	X	O	O	X	-	-	-	-	-	-	-	-
06MN07a	X	X	-	-	X	-	-	-	-	-	-	-	-
06MN07b	X	-	X	-	X	-	-	-	-	-	O	-	-
06MN08	X	-	-	-	-	-	-	-	X	-	-	X	O
06MN10	X	O	O	-	X	-	-	-	-	-	-	-	-
06MN11	X	O	-	-	X	-	-	-	-	-	-	-	-
06MN12	X	O	X	-	X	-	-	-	-	-	O	-	-
06MN13	X	X	O	T	X	O	O	O	-	-	T	-	-

Table 1. Mineral assemblages of samples cut into thin sections from the Montagne Noire Gneiss Dome. Mineral name abbreviations: QZ – quartz, PL – plagioclase, MUS – muscovite, CHL – chlorite, BI – biotite, GT – garnet, ST – staurolite, S – sillimanite, CA – calcite, OP – opaques, TO – tourmaline, EP – epidote, CP – clinopyroxene.

X > 10%, O = 1-10%, T < 1%, - not present

pyrite, kaolinite, and tourmaline. Evidence of calcite growth in equilibrium with dolomite is seen in Figures 10 and 11. Figure 10 also shows three growths of calcite. The first growth is Mg-rich (Carb7) while the second growth (Carb8) plots in the middle of and just above the dolomite-ankerite tie line and the third growth (Carb9) plots halfway between the first two growths. No grains are larger than 500  $\mu\text{m}$  in this calc-silicate. An unusual characteristic of 06MN15a is the pervasive growth of fibers of an unknown mineral (tremolite?) that can be found growing in groups over plagioclase and quartz. In many locations the fibers grow over grains of muscovite. Sample 06MN16aA is gneissic-schist with perthite and myrmekite. Sample 06MN18A is from the core of L'Espinouse and is quartzo-feldspathic gneiss with a discontinuous foliation defined primarily by biotite.

#### *Col de Pierre Plantée*

Nine samples were collected and made into thin sections from the Col de Pierre Plantée (Table 1 and Figure 3). Except for tourmaline, individual grains in the phyllites are too fine-grained to distinguish. Micaceous band thickness and the length and degree of curvature of these bands vary between the samples. XRD analyses of sample 32 shows peaks congruent with clinochlorite. Sample 06MN22A is highly sheared. Sample 06MN38A has feldspar sigma-clasts consistently indicating a top-to-the east sense of shear (Figure 12).

#### **Rosis Syncline**

Thin sections were made from five samples from the Rosis syncline (Fig.1), which divides L'Espinouse to the north and Le Caroux to the south. Except for sample

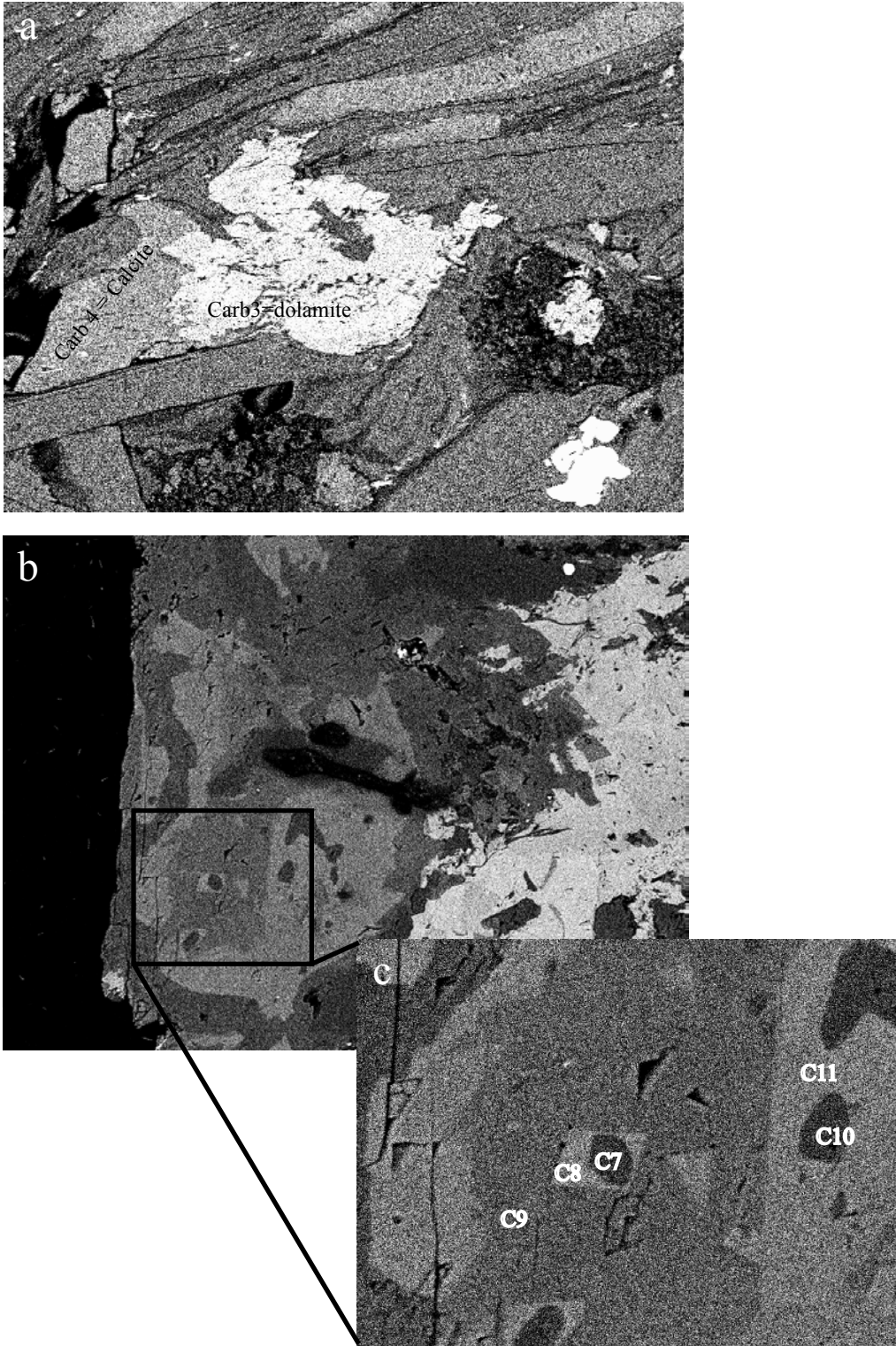


Figure 10. Backscattered electron images of sample 06MN15a from the Caroux transect in L'Espinoise. Lighter regions represent higher mean atomic number. (a) Calcite growing in equilibrium with dolomite. (b) Three different compositions of calcite. (c) Close-up of (b) showing labelled analyses to be compared compositionally on Figure X.

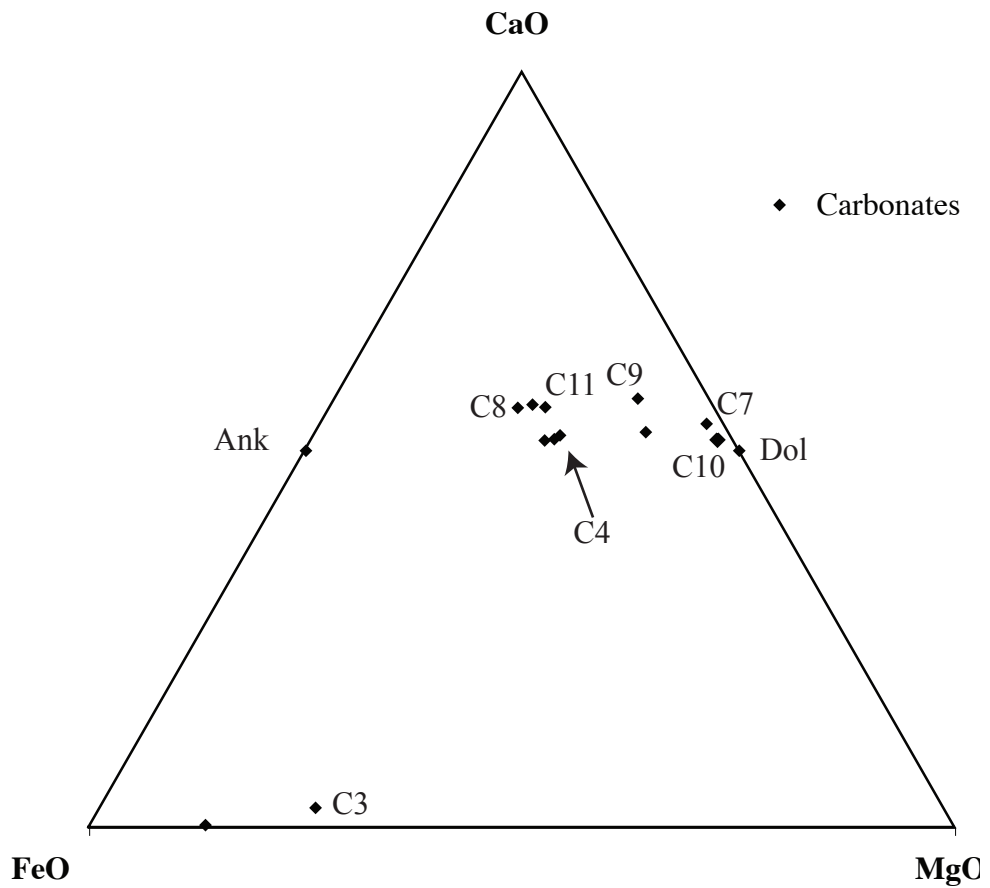


Figure 11. Compositions of carbonates from sample 06MN15a plotted with CaO, FeO, and MgO axes. Ankerite (Ank) and dolomite (Dol) plotted for reference. C3 and C4 are in contact and suggests that this rock may have been reset at very low temperatures, as suggested by Essene (1983). C7 grew followed by C8 and C9.

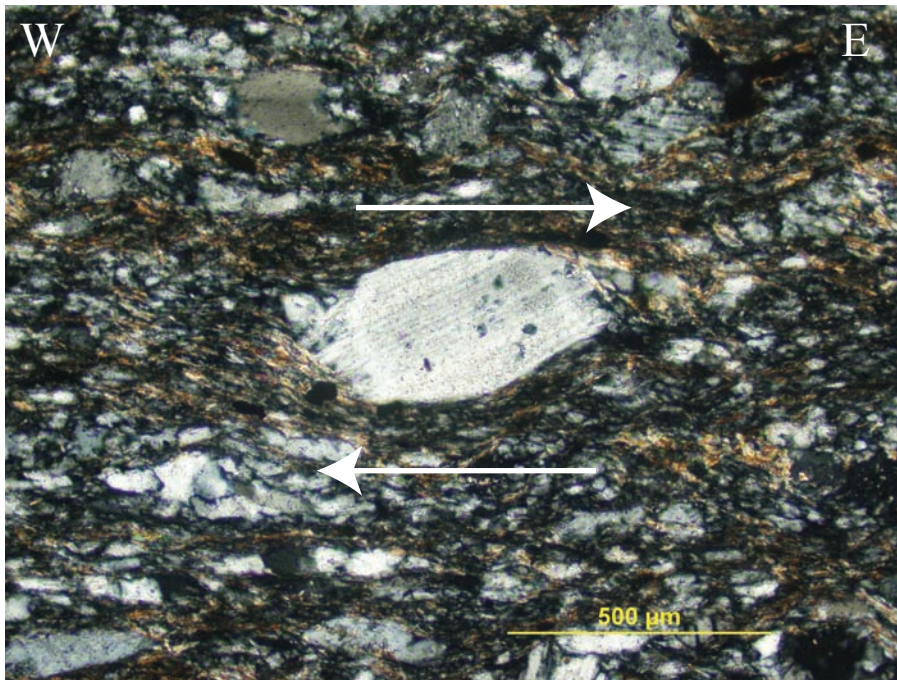


Figure 12. Photomicrograph in xpl of a plagioclase sigma clast from 06MN38A. This shows a top-to-the east shear sense.

06MN09A, which is a migmatite, all of the samples are schists with well-defined foliations. Biotite is more abundant than muscovite in the samples that contain both biotite and muscovite. Fibrolite is present in 06MN28A and in 06MN09A; the grungy masses in the migmatite may be sillimanite, cordierite, or altered plagioclase. The migmatite also contains perthite, which may have formed as the sample cooled to temperatures below 675 °C (Winter, 2001 and references within). Sample 27 is the westernmost sample containing muscovite that was collected from this region.

### **Le Caroux**

Thin sections were made from eleven samples collected from the metasedimentary envelope of Le Caroux subdome (Figure 3 and Table 1). All of the samples, with the exceptions of 06MN01c and 06MN08a, which are calc-silicates, are schists. Grain sizes range between 50 µm - 3mm, but quartz and plagioclase are invariably the largest grains in every sample. Feldspar porphyroblasts are abundant in 06MN12aA and an apatite porphyroblast with quartz and feldspar pressure shadows is prominent. Staurolite porphyroblasts are present in 06MN02aA and indicate a top-to-the east sense of shear. Quartz pressure shadows are evidence that growth of a staurolite porphyroblast preceded the deformation pulse or event during which the pressure shadows grew (Figure 13) (Winter, 2001). Staurolite and garnet porphyroblasts are highly fractured and elongate. Sample 06MN03A has exceptionally large, euhedral grains of staurolite and garnet ranging from 0.5-5 mm in length for the staurolite and 1-2.5 mm in diameter for the garnet. One pair of grains is separated by a small, fibrous mass (Figure 14). The garnet in Figure 14 has quartz inclusion trails that define  $S_2$  and are abruptly truncated by new

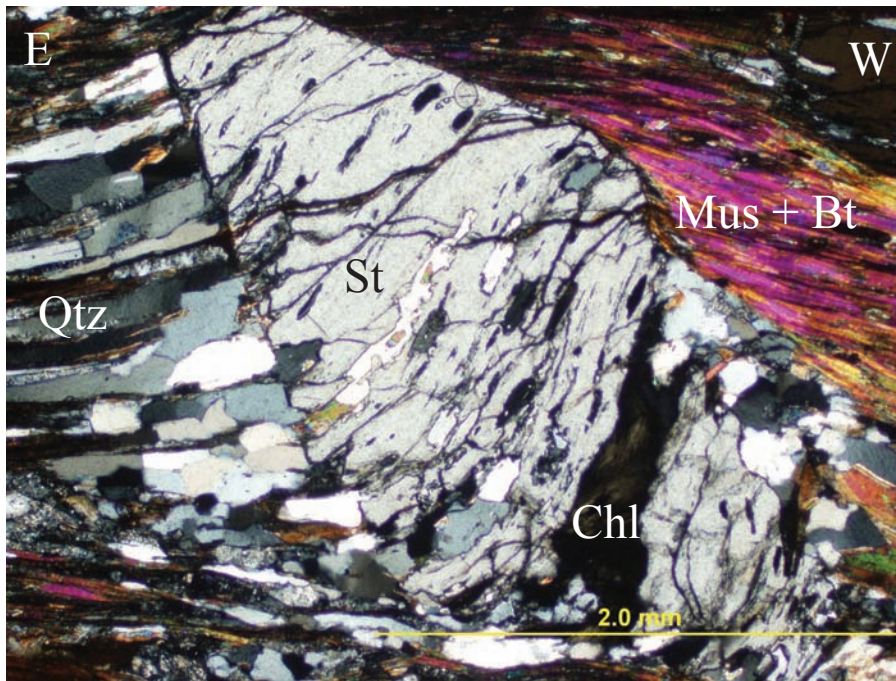


Figure 13. Photomicrograph in xpl of a staurolite (St) porphyroblast partially altered to chlorite (Chl) along a fracture. Quartz (Qtz) pressure shadows are evidence that growth of the staurolite crystal preceded the metamorphism during which the pressure shadows grew.



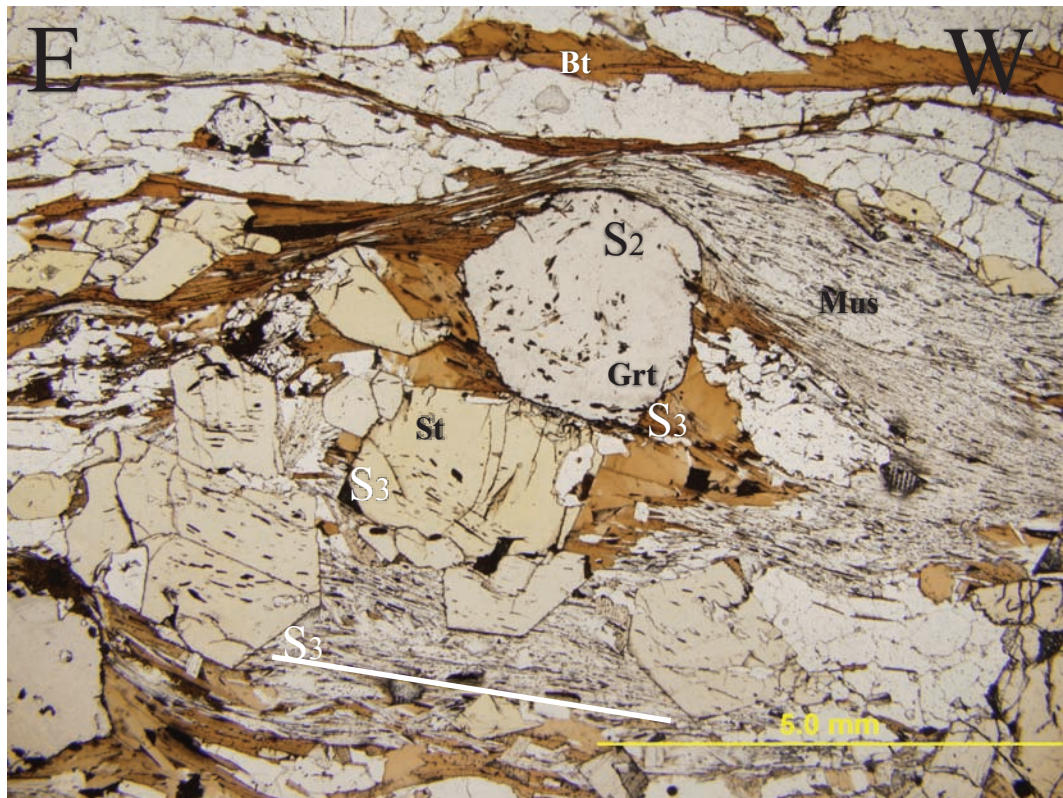


Figure 14. Photomicrograph in ppl of sample 03 from Le Caroux. Quartz inclusions in garnet and staurolite define a succession of cleavages. Abbreviations are as follows: Grt = garnet, St = staurolite, Mus = muscovite, Bt = biotite.

growth of a Mg-rich garnet rim. In sample 13, cleavages S1 and S3 are orthogonal to S2 in the plane parallel to lineation and perpendicular to the most recent foliation (Figure 15). This clearly indicates that at least three deformational pulses or events occurred during the formation of this schist. The two cleavages, S2, and S3, in sample 03 are also orthogonal to each other in the plane parallel to lineation and perpendicular to the most recent foliation. S2 and S3 in sample 03 have the same orientations, as S2 and S3 in 13. It is possible that the corresponding cleavages between samples 03 and 13 represent the same cleavages and thus the same deformation pulses or events.



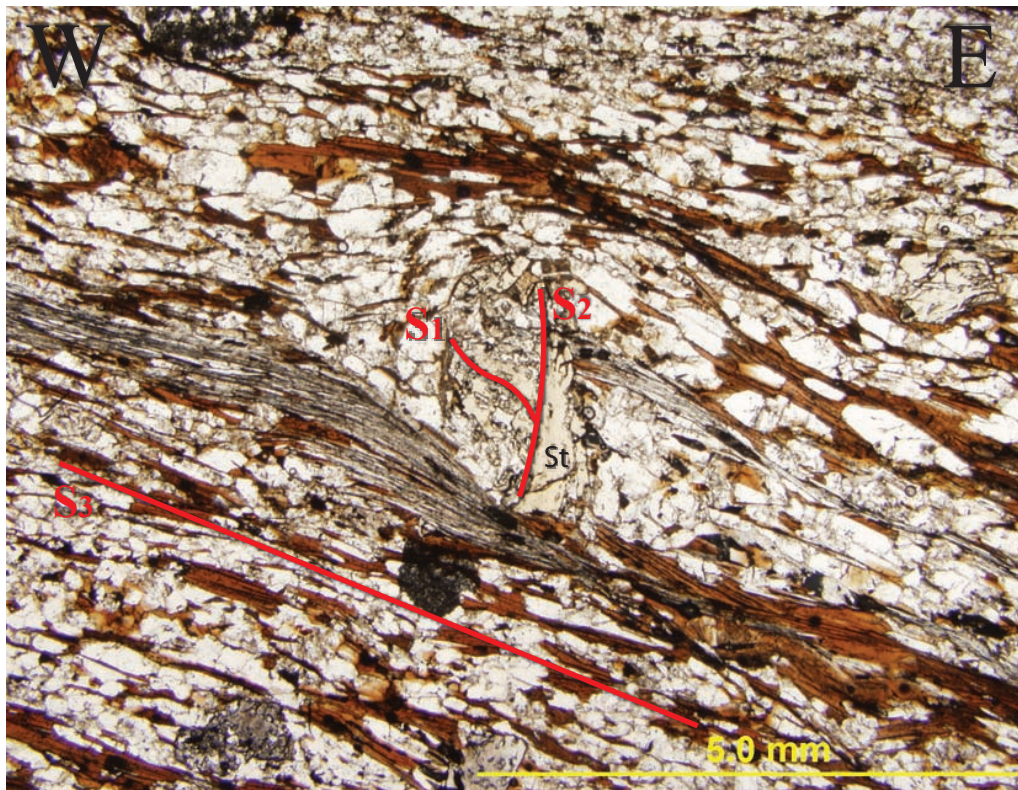
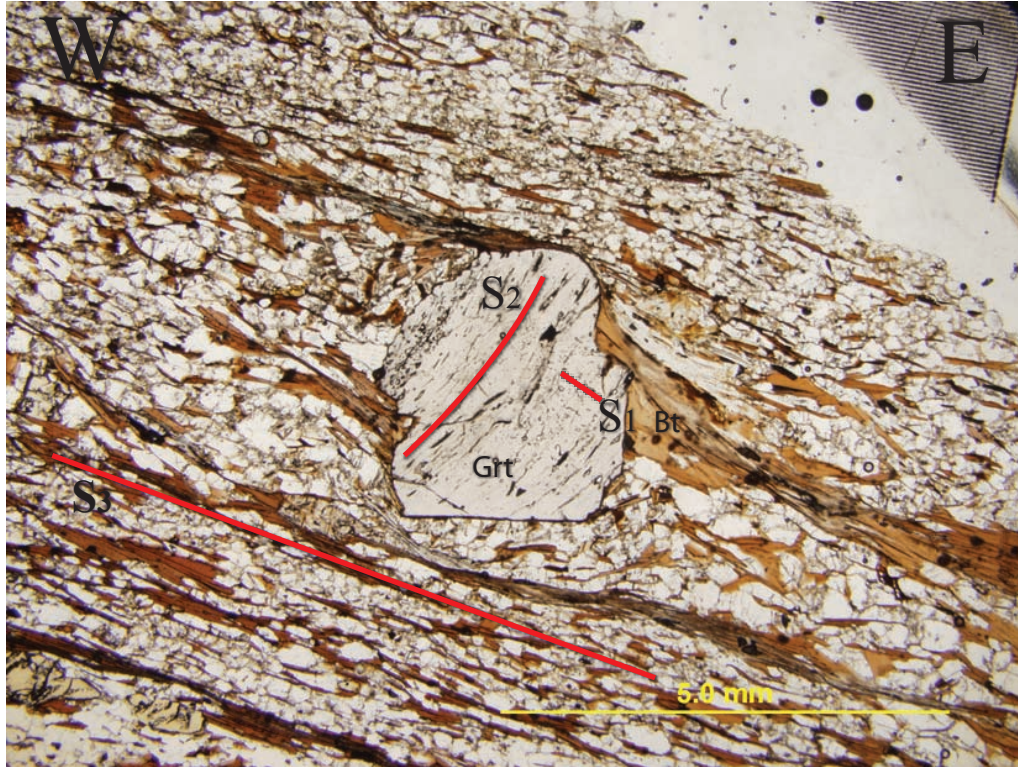


Figure 15. Photomicrographs in ppl of oriented thin sections of sample 06MN13. S1, S2, and S3 correspond to cleavage directions that are pervasive in the sample.

## GEOTHERMOBAROMETRY

### **Methods**

The mineral compositions for seven thin sections representing seven distinct samples were obtained using the JEOL JSM 6400 Scanning Electron Microscope at Smith College. The samples were polished to a 1-micron diamond grit and coated with a thin layer of carbon. All quantitative analyses were performed under operating conditions of 20kV accelerating voltage and a beam current of  $2.61 \pm .01$  nA. Quantitative analyses of garnet, biotite, muscovite, plagioclase, feldspar, staurolite, and tourmaline were performed using the Oxford Link ISIS Energy Dispersive X-Ray Microanalysis system and a Quant Calibration was performed every two hours using a Cobalt Standard.

The metamorphic pressure-temperature conditions of the analyzed samples were determined using several programs. The principal program used was GTB (Kohn and Spear, 2001). All analyses used the garnet-biotite Fe-Mg exchange thermometer without any correction for  $\text{Fe}^{3+}$ , and the Ferry and Spear ideal biotite solution model combined with the Berman (1990) garnet calibration. The garnet-plagioclase-muscovite-biotite barometer with the Hodges and Crowley (1985) calibration was also used unless otherwise stated. Analyses of chemical compositions for the inner and outer cores were obtained for garnets because some of the garnets are zoned. The outer core garnet compositions were used with compositions from biotite grains in contact with the garnet for the garnet-biotite exchange thermometer and the garnet-biotite-plagioclase-muscovite and garnet-biotite-plagioclase-quartz barometers. These analyses were chosen in an attempt ensure equilibrium between the garnet and the biotite. This approach may not

yield maximum temperatures of metamorphism due to Fe-Mg exchange between garnet and biotite during cooling.

## **Results**

Five samples were analyzed for geothermobarometry from Le Caroux. Sample 01b, a garnet schist, was collected in unit X<sub>6</sub> from the southeastern end of Le Caroux and yields a temperature of  $550 \pm 25$  °C and a pressure of  $6 \pm 0.5$  kbar (Figure 16). The garnet-plagioclase-biotite-quartz barometer with both the Hoisch (1990) Mg-R1 and Hoisch (1990) Fe-R2 calibrations was used in the absence of muscovite. Again this barometer and these calibrations were used for Sample 02a, a garnet-staurolite schist, which is also from the unit X<sub>6</sub> and was collected 200 m northwest of Sample 01b. Temperatures and pressures derived using GTB are  $500 \pm 50$  °C and 3 kbar, respectively (Figure 16). The barometry is inconclusive because only one barometric analysis was obtained. However, the garnets in 02a are Fe-rich and the 2000 unpublished Spear and Cheney petrogenetic grid for pelites (Figure 17) predicts pressures above 3.0 kbar, respectively. The presence of staurolite indicates  $T > 500$  °C. Sample 03, a garnet-staurolite schist from unit X<sub>5</sub> just 400 m northwest of sample 02a in Le Caroux, shows a similar temperature of  $560 \pm 20$  °C but a higher pressure at  $8 \pm 1$  kbar (Figure 13). Sample 13a is also a garnet-staurolite schist from unit X<sub>4</sub> with the addition of fibrolite, but is from the northeast end of Le Caroux. The temperature is  $575 \pm 25$  °C and the pressure is  $6.25 \pm 0.75$  kbar (Figure 18). These temperatures and pressures are similar to those from sample 01b. The pressure could not be determined for sample 12, the westernmost sample collected in Le Caroux,

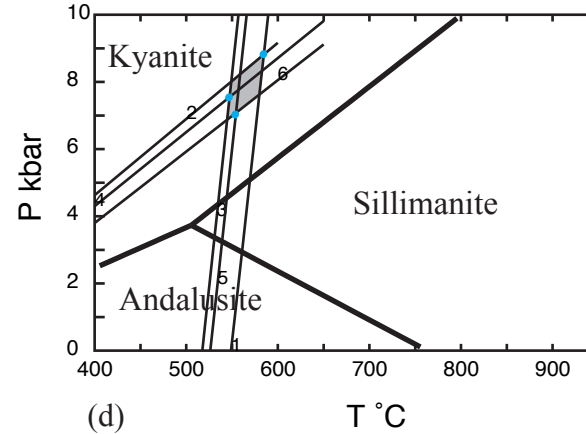
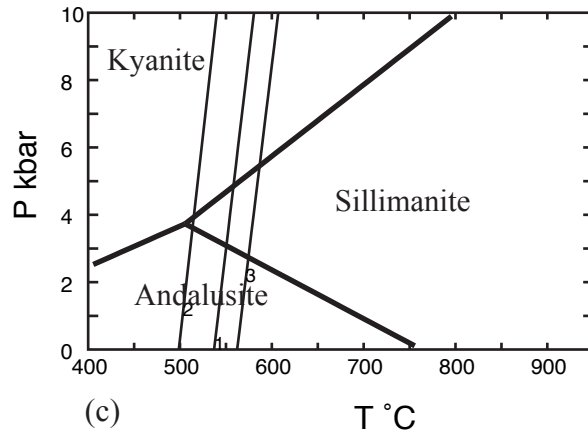
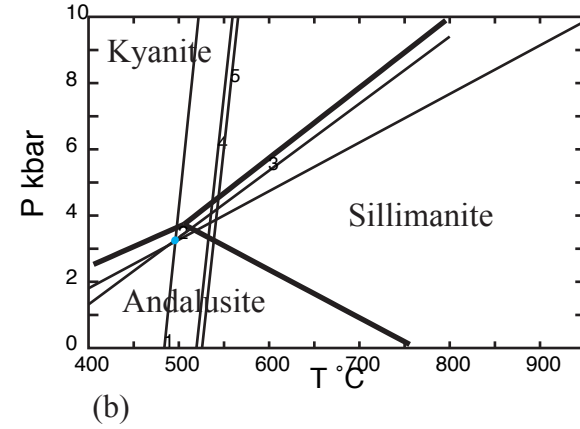
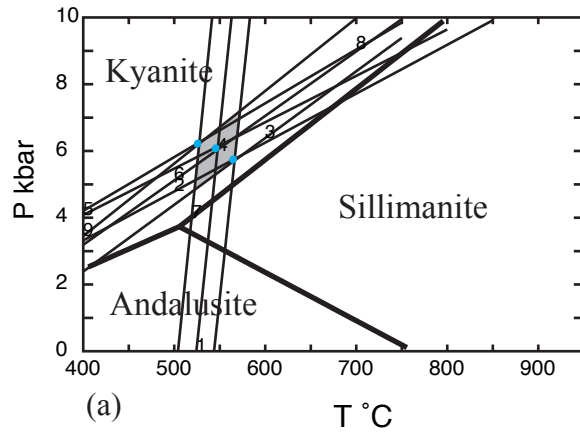


Figure 16. P-T diagrams derived from GTB (Kohn and Spear, 2001) for samples (a) 01b, (b) 02a, (c) 12a, and (d) 03 from Le Caroux. Grey regions represent the range of P-T conditions and blue points represent individual analyses.





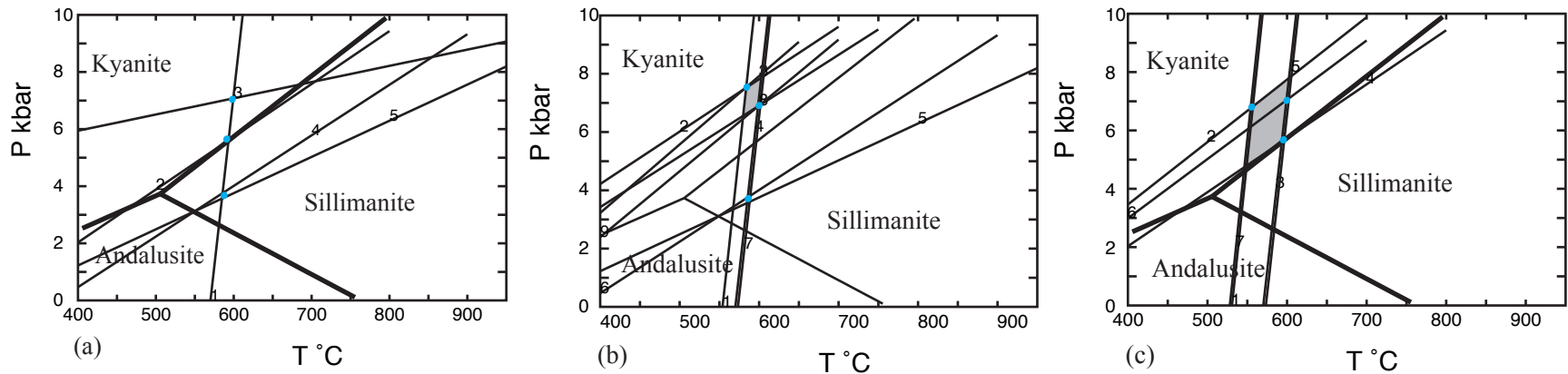


Figure 18. P-T diagrams generated from GTB (Kohn and Spear, 2001) for sample 13a. (a) Check for internal consistency of temperature using gar-bt-plag-qtz with the Hoish Fe and Hoish Mg (1990) calibrations and gar-bt-plag-mus barometers with Holland and Powell (1988) calibration and Hodges and Crowley (1985) calibration, (b) gar-bt-plag-qtz barometer, and (c) gar-bt-plag-mus barometer with the Hodges and Crowley (1985) calibration. Grey regions represent the range of pressures and temperatures and blue points are individual analyses.



but again the temperature recorded in the biotite-tourmaline thermometer is  $550 \pm 50$  °C (Figure 16).

The Rosis Syncline and L'Espinouse did not provide samples conducive to geothermobarometric analysis. A muscovite-biotite schist (27a) from the Rosis Syncline shows a temperature of  $575 \pm 50$  °C and a biotite-schist (32a) from the easternmost end of L'Espinouse shows a temperature of  $500 \pm 25$  °C (Figure 19). These temperatures were obtained using a biotite-tourmaline thermometer with the Colo and Fri (1987) + Delta V calibration.

The program Thermobarometry with Estimation of Equilibrium State (TWQ v.2.3.2) was also used. This program uses internally consistent thermodynamic data for endmembers and solid solution phases. The Berman & Aranovich (1996, CMP, 26, 1-24) garnet model was used with the biotite model outlined in the TWQ documentation (2007). Pressure and temperature conditions obtained using TWQ and the assemblages in Figure X are similar to those obtained using GTB. TWQ yielded pressures and temperatures of 500 °C and 7.5 kbar, for sample 03A (Figure 20) and 550 °C and 5 kbar for sample 02a (Figure 21). These pressures and temperatures are similar to those obtained using GTB. Pressure was not constrained for sample 01b, but the temperature yielded was  $575 \pm 25$  °C as defined by the garnet-biotite Fe-Mg exchange thermometer (Figure 22).

Garnet is Fe-rich. The Mg, Mn, and Ca contents are variable in sample 03A, but samples 01b, 02a, and 13a have equivalent amounts. Garnet 2 in sample 03A exhibits growth zoning, as shown by a decrease in Mn and Ca from core to near-rim (Figure 23). Mn preferentially partitions into garnet, which is why the garnets have high Mn cores.

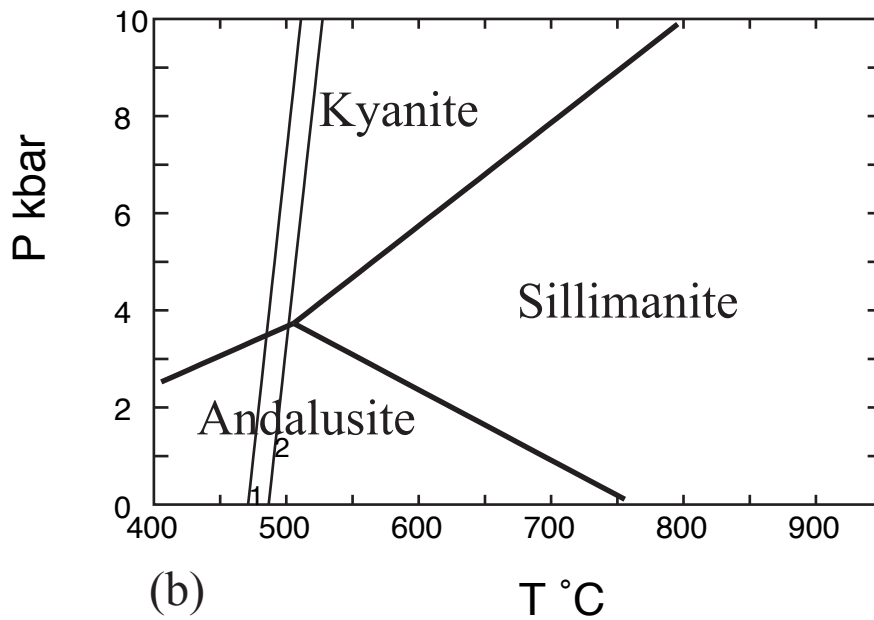
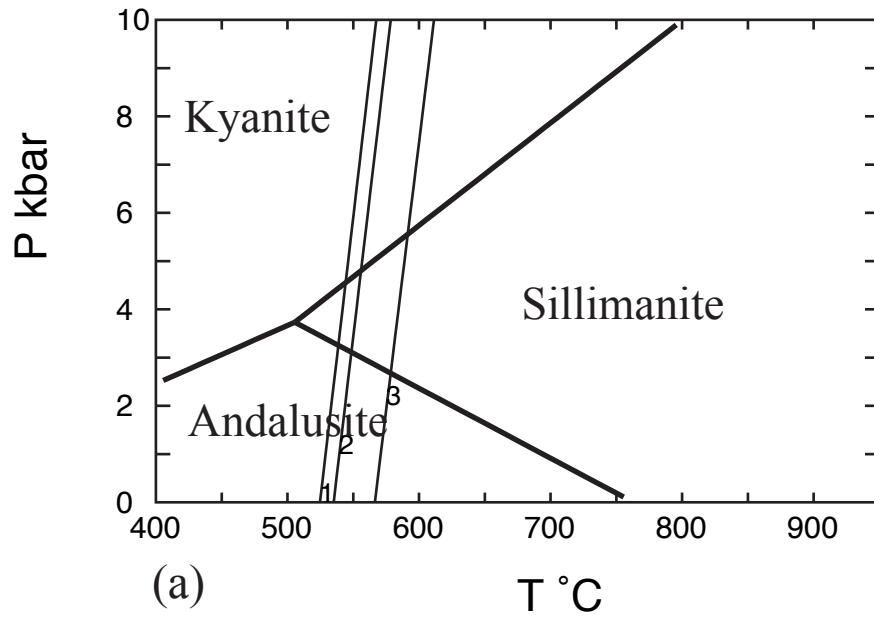


Figure 19. P-T diagrams derived from GTB (Kohn and Spear, 2001) for samples (a) 27a (b) 32a from L'Espinoise. The biotite-tourmaline thermometer with the Colo and Fri (1987) + Delta V calibration was used.

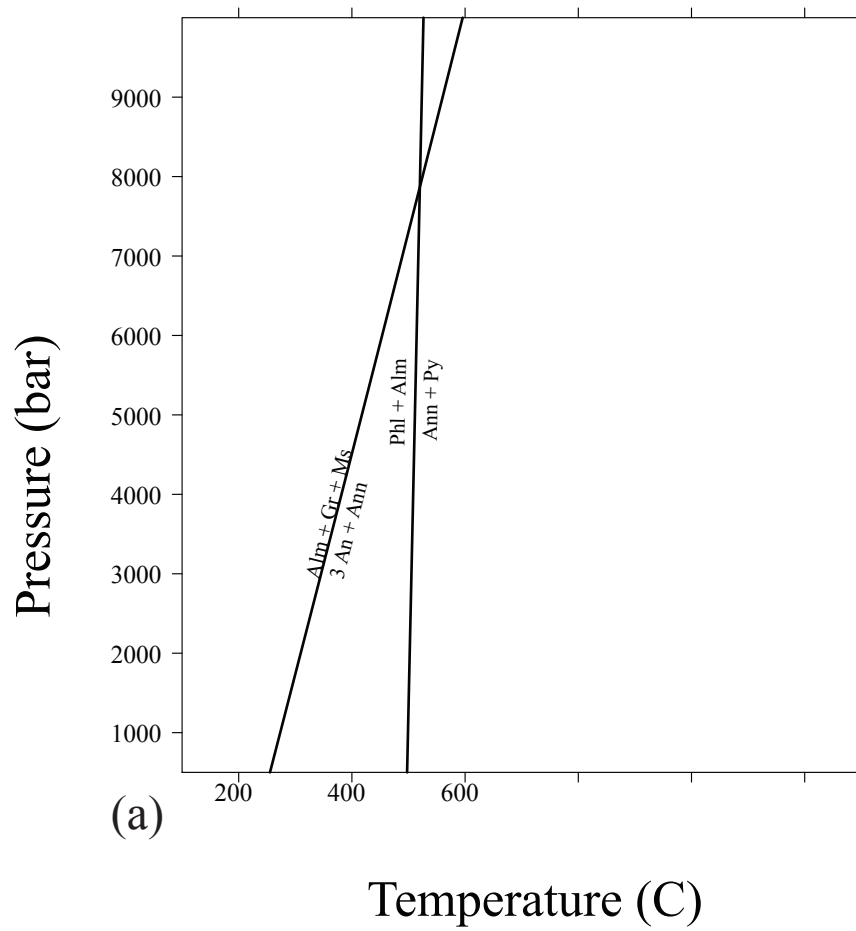


Figure 20. P-T graphs constructed using TWQ for sample 03 from Le Caroux using suggested reactions.

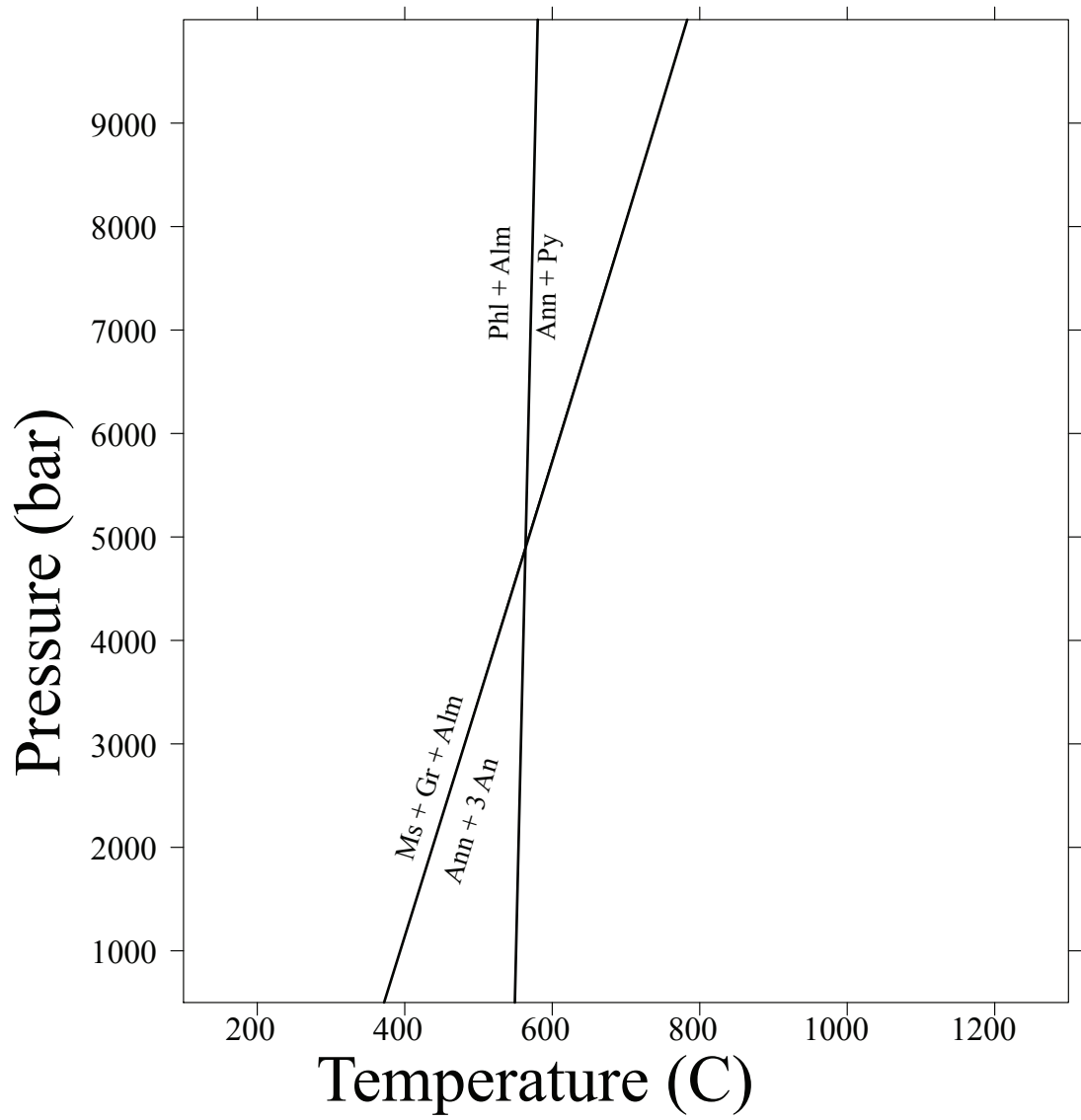


Figure 21. P-T graph constructed using TWQ for sample 02a from Le Caroux.

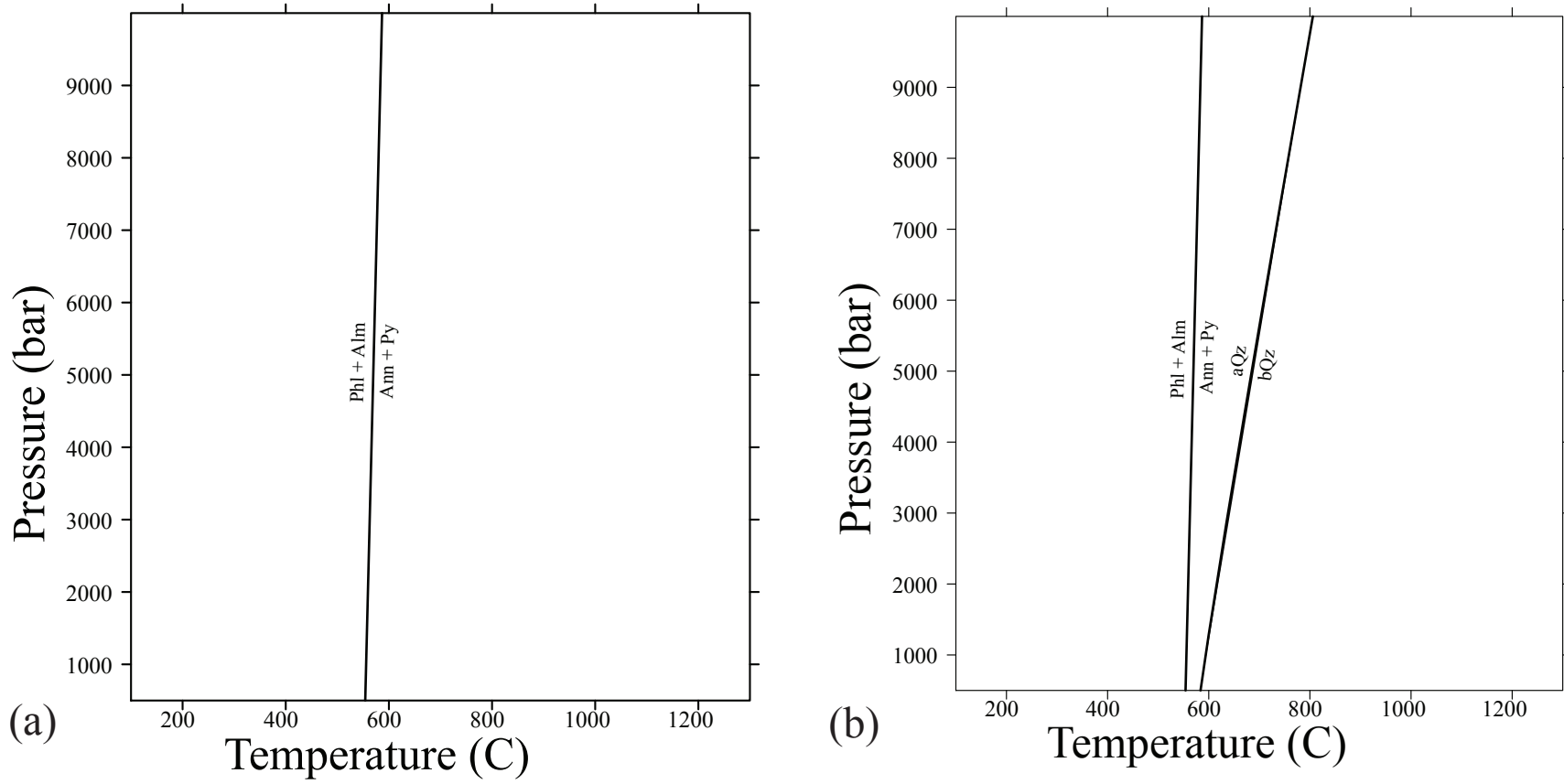


Figure 22. P-T graphs constructed using TWQ for sample 01b from Le Caroux; (a) suggested reactions and (b) all reactions.

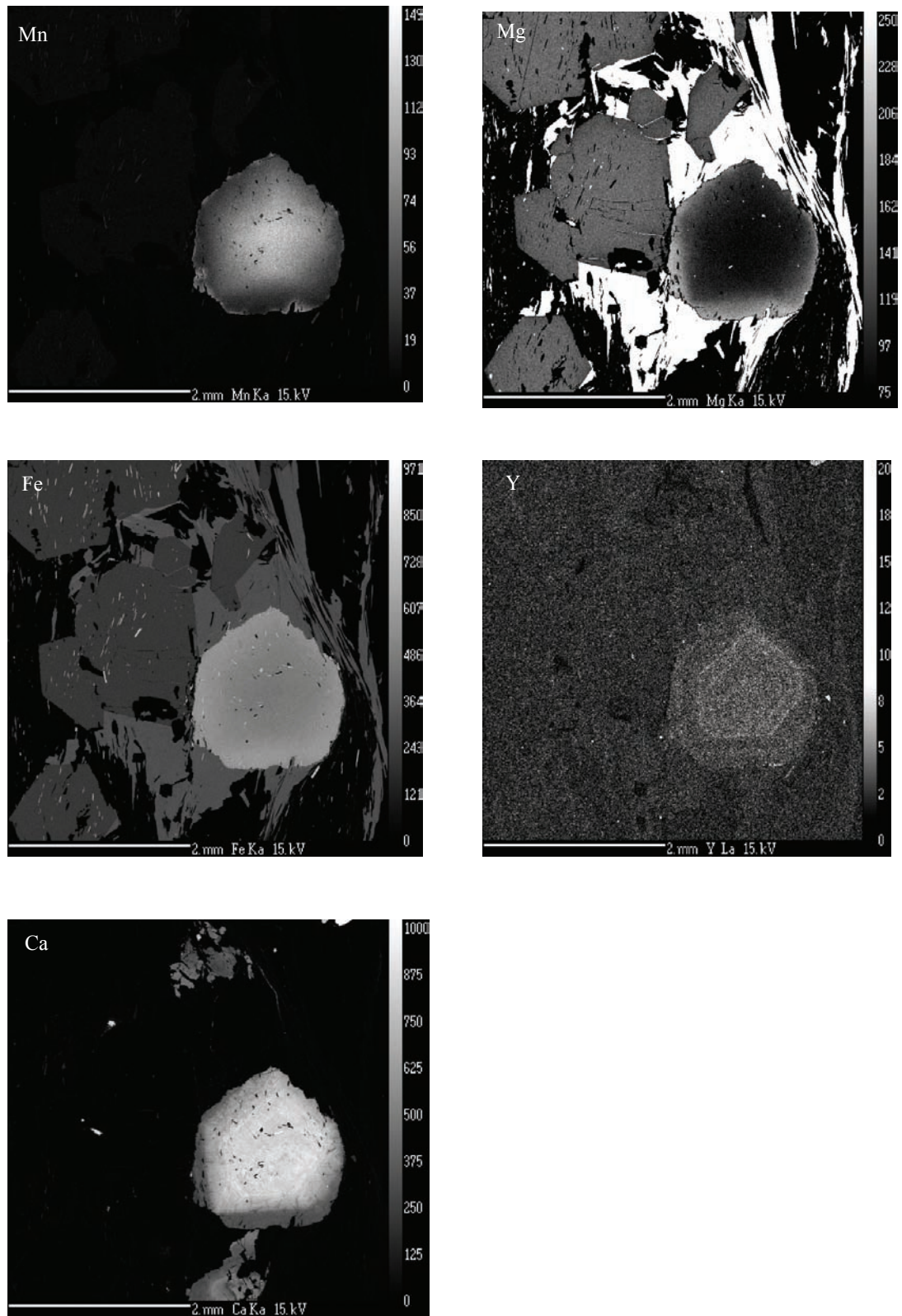


Figure 23. Element maps for garnet 1 from thin section 03A from Le Caroux. These maps illustrate the Mn, Ca, and Y depleted troughs and the outer rim of increased Mn. The Mn rim may be the result of garnet dissolution that led to a net-transfer reaction.

An increase in Mn defines a discontinuous outer rim that is thinner than the diameter of the electron beam, which does not allow us to quantify this increase. The high-Mn rim may have formed during partial dissolution (resorption) of the garnet rim (Kohn and Spear, 2000). This implies, “(1) the garnet was once larger, and had a uniformly low Mn content towards its rim. (2) the garnet dissolved during cooling and exhumation returning Mn to the matrix, and (3) because biotite contains negligible Mn compared to garnet, Mn increased on the rim of the garnet and back-diffused into the garnet” (Kohn and Spear, 2000). Although some garnet dissolution occurred, it is unlikely that any net transfer reactions significantly changed the compositions of the garnets and biotites. Because I used garnet analyses from the outer core and not from the high-Mn rim, it is unlikely that the calculated temperatures are higher than the peak temperatures reached during metamorphism. It seems more likely that some re-equilibration took place during retrograde metamorphism and that the calculated temperatures are slightly below peak temperatures.

Samples 01b, 02a, 03, 12, and 13 from Le Caroux yield temperatures and pressures of  $550 \pm 25$  °C and  $6 \pm 0.5$  kbar,  $500 \pm 50$  °C and 3 kbar,  $560 \pm 20$  °C and  $8 \pm 1$  kbar,  $550 \pm 50$  °C, and  $575 \pm 25$  °C and  $6.25 \pm 0.75$  kbar, respectively. Overall, the metamorphic grade increases from the east to the west in the metasedimentary envelope of Le Caroux. Sample 27a from the Rosis Syncline yields a temperature of  $575 \pm 50$  °C and sample 32a from the easternmost end of the metasedimentary envelope of L’Espinoise yields a temperature of  $500 \pm 25$  °C.

## MONAZITE DATING

### **Methods**

Two samples were selected from unit X<sub>5</sub> in Le Caroux for monazite dating. Sample 13A is from the north of the subdome and 03A is from the south (Figure 3). The samples were sent to The University of Massachusetts at Amherst where Professors Michael Jercinovic and Michael Williams processed them. Full section maps in Ce and Mg were made; Ce is concentrated in monazites and is used to identify monazite grains and Mg is used as a reference element for the base map. The thin section was then cleaned, re-polished with a silica vibrational polish and coated under a vacuum with ~200Å Al followed by ~80 Å C. Monazite grain maps in Ca, Pb, Th, U, and Y were made for selected monazite grains. Based on these maps, several grains from each sample were chosen for analysis. Background scans for trace element analyses in each domain in each grain were run followed by the trace element analyses. The program DatCon, developed by Michael Williams and Michael Jercinovic, was then used to obtain ages after careful scrutiny of individual analyses. Michael Jercinovic processed all of the data reduction and subtracted background intensities following the procedure outlined in Williams et al. (2006). See the UMass website for additional information about procedures and monazite dating (<http://www.geo.umass.edu/probe/Monazite%20techniques.htm>).

### **Results**

Five grains were analyzed in sample 13. The analyses from m7 were all targeted at the core of the monazite grain (Figure 24) yielding the age  $352 \pm 4.1$



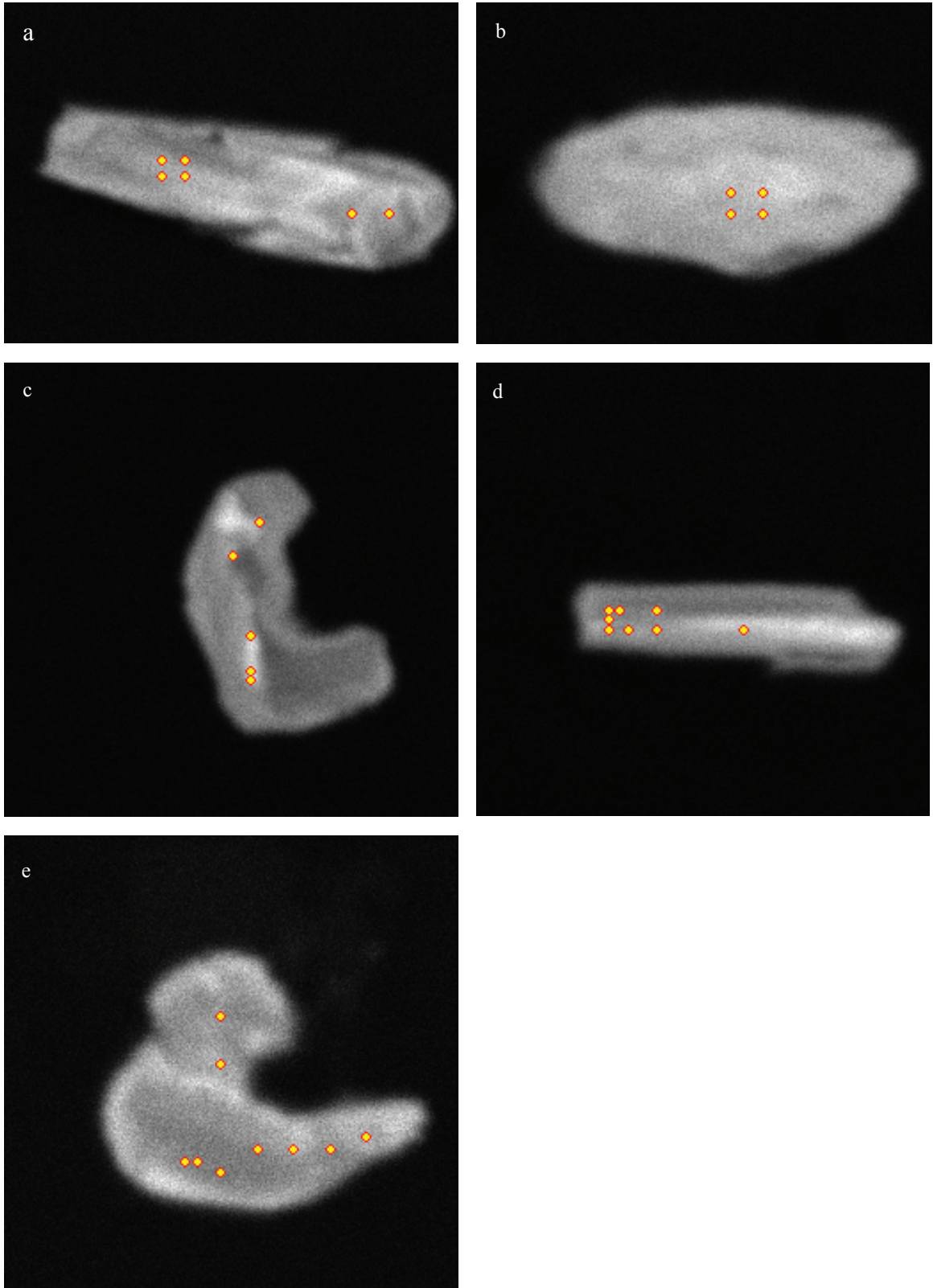


Figure 24. Th maps of monazite grains from sample 13 with the points of analysis. The monazite grains are as follows: (a) m2, (b) m3, (c) m4, (d) m5, and (e) m7.

Ma. M3 yielded an age of  $328 \pm 2.7$  Ma. The ages from grains m2, m4, and m7 are  $310 \pm 3.2$  Ma,  $314 \pm 2.0$  Ma, and  $313 \pm 3.3$  Ma, respectively. The Th-zoning in these grains was mottled (Figure 24), but all analyses attempted to capture the high Th areas.

Compared to m7, the compositions for grains m2, m4, and m5 were all high in Ca, Th, Sm, and Tb and low in La and Dy (Figure 25). I propose that the high-Th cores in m2, m4, and m5 all grew during the same stage of metamorphism based on their similar chemical compositions and the clustering of ages. The weighted average for these three grains is  $312 \pm 6$  Ma. Figure 26 shows a histogram of ages from each domain that was analyzed in sample 13.

Five monazite grains in sample 03A were analyzed. The domains within the individual grains are mainly defined by differences in Th levels, although a U-defined domain in m9 was sampled (Figure 27). M2 is a small grain with narrow domains (Figure 28). The calculated age is  $309 \pm 2.3$  Ma. M4 is actually two grains, an upper and a lower grain. Analyses in the low-Th upper domain yielded the age  $326 \pm 4.4$  Ma while the high-Th age is  $281 \pm 3.9$  Ma. Unfortunately, the domains are mottled and it is not possible to distinguish a core and rim. The low Th domain in the lower m4 grain yielded an age of  $347 \pm 4.1$  Ma. The low-Th core and high-Th rim in m7 yielded ages  $388 \pm 6$  Ma and  $288 \pm 3.0$  Ma, respectively. The clearly defined domains and significant age difference indicate that the domains grew during different metamorphic events. The high-Th domain in the core and the high-U crescent domain on the rim of m9 were analyzed and yielded ages of  $301 \pm 2.3$  Ma and  $307 \pm 3.8$  Ma, respectively (Figure 28). It is unlikely that these ages represent two distinct metamorphic events because the ages are so closely clustered. The ages are very close and the Th domains within m9 are not well

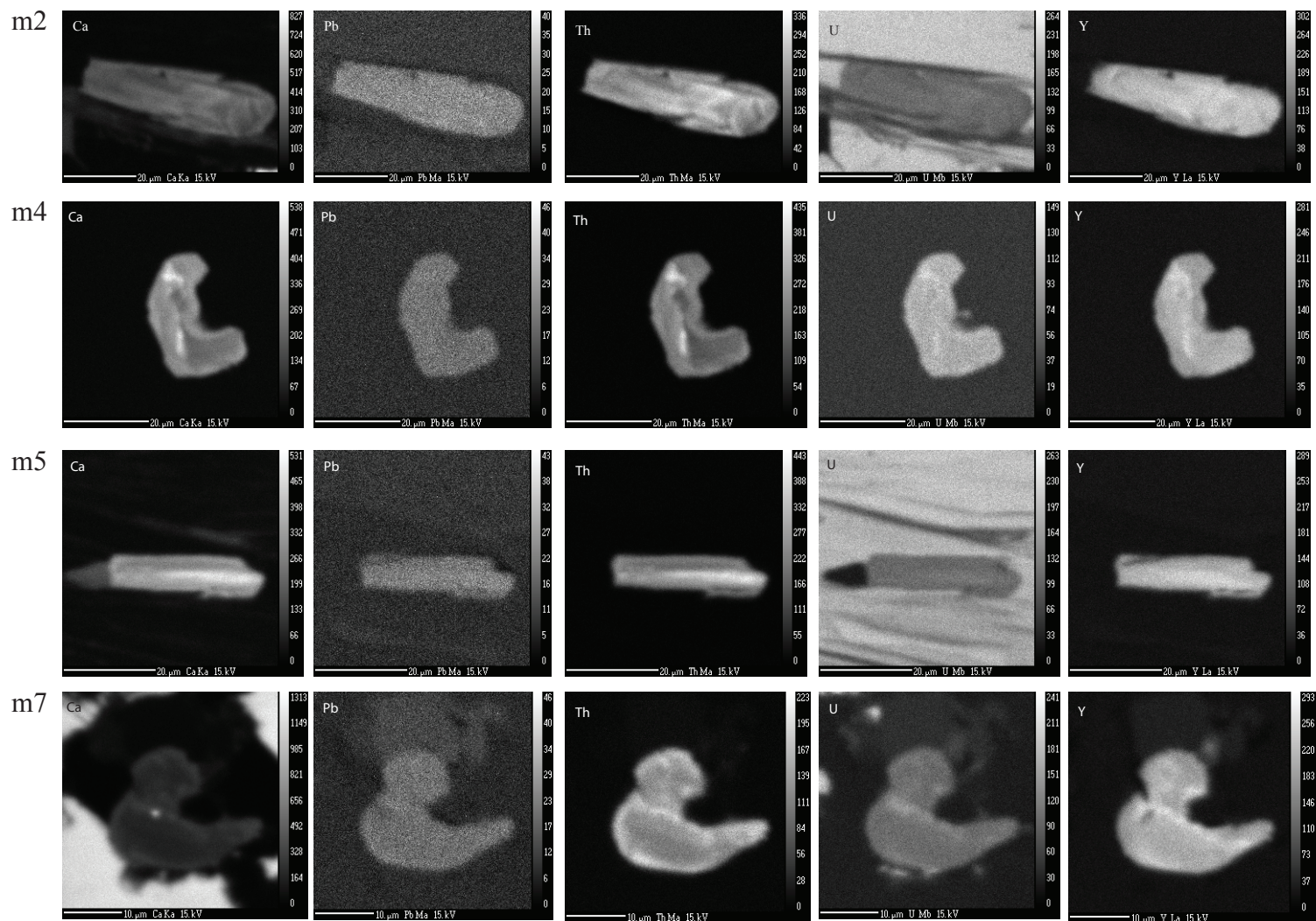


Figure 25. Compositional maps of monazite grains in sample 13 from the UMass microprobe.

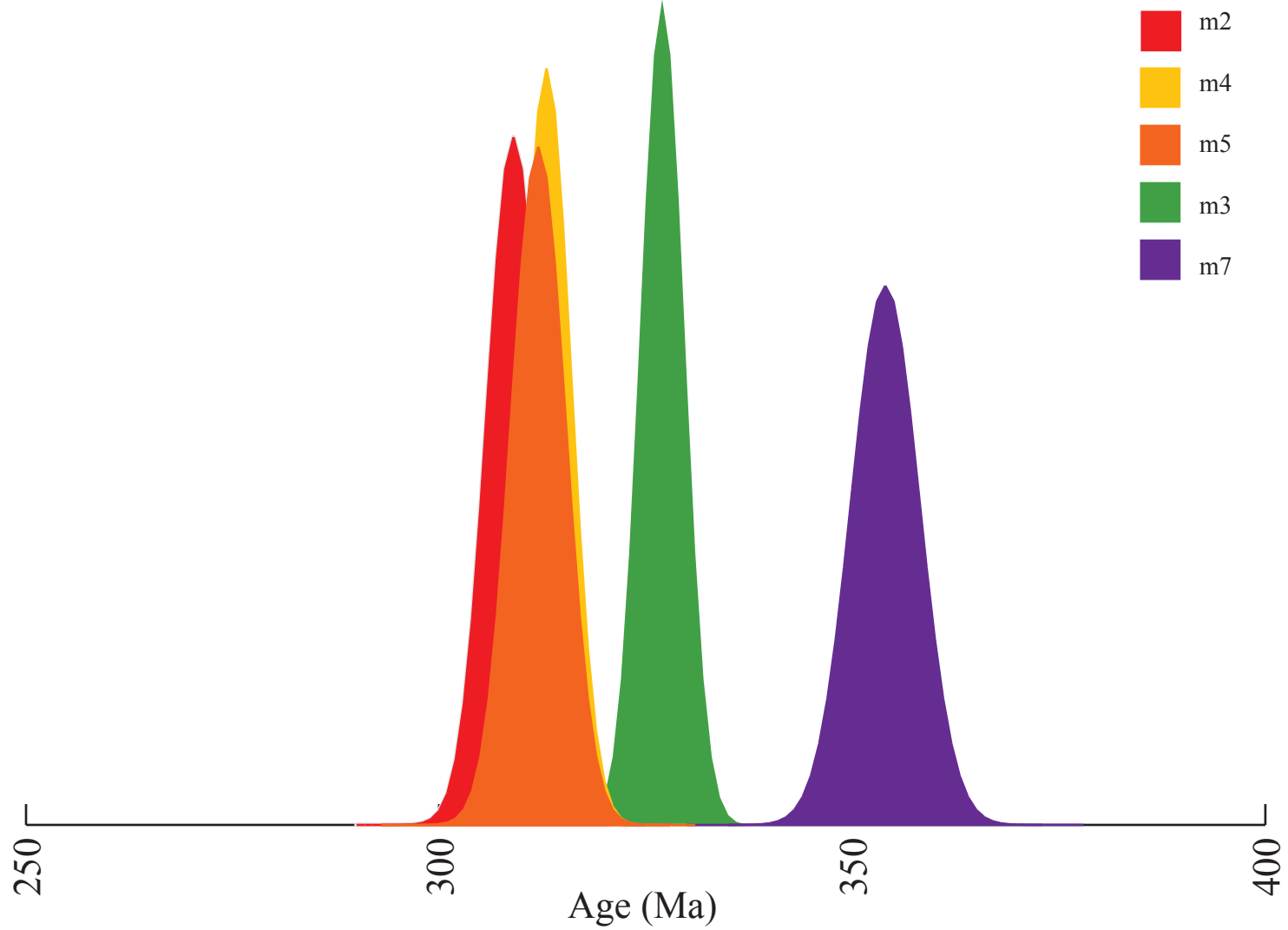


Figure 26. Histogram of ages of monazite growth from sample 13 with a clustering at 312 Ma.



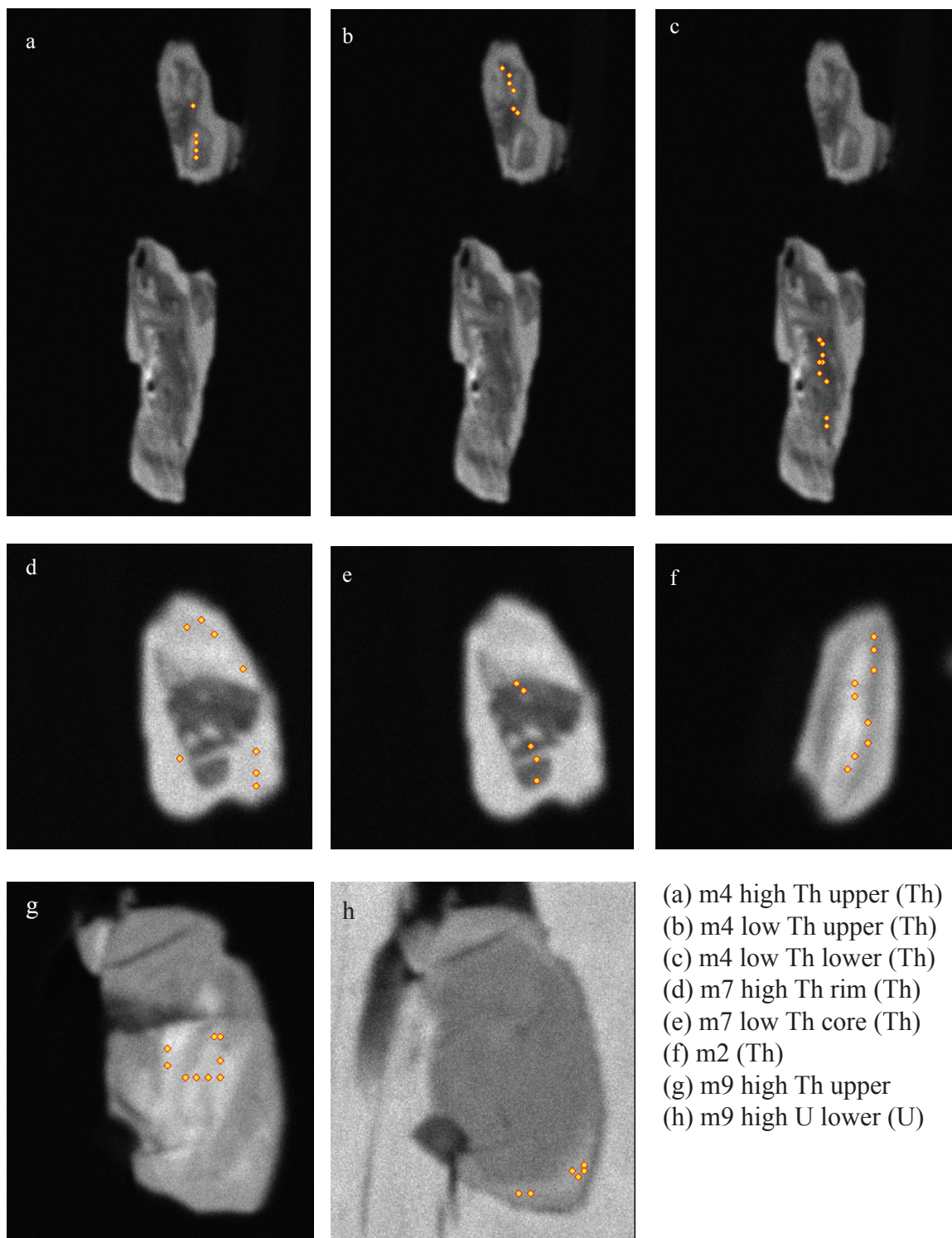


Figure 27. Th and U maps of monazite grains from sample 13 with the points of analysis.

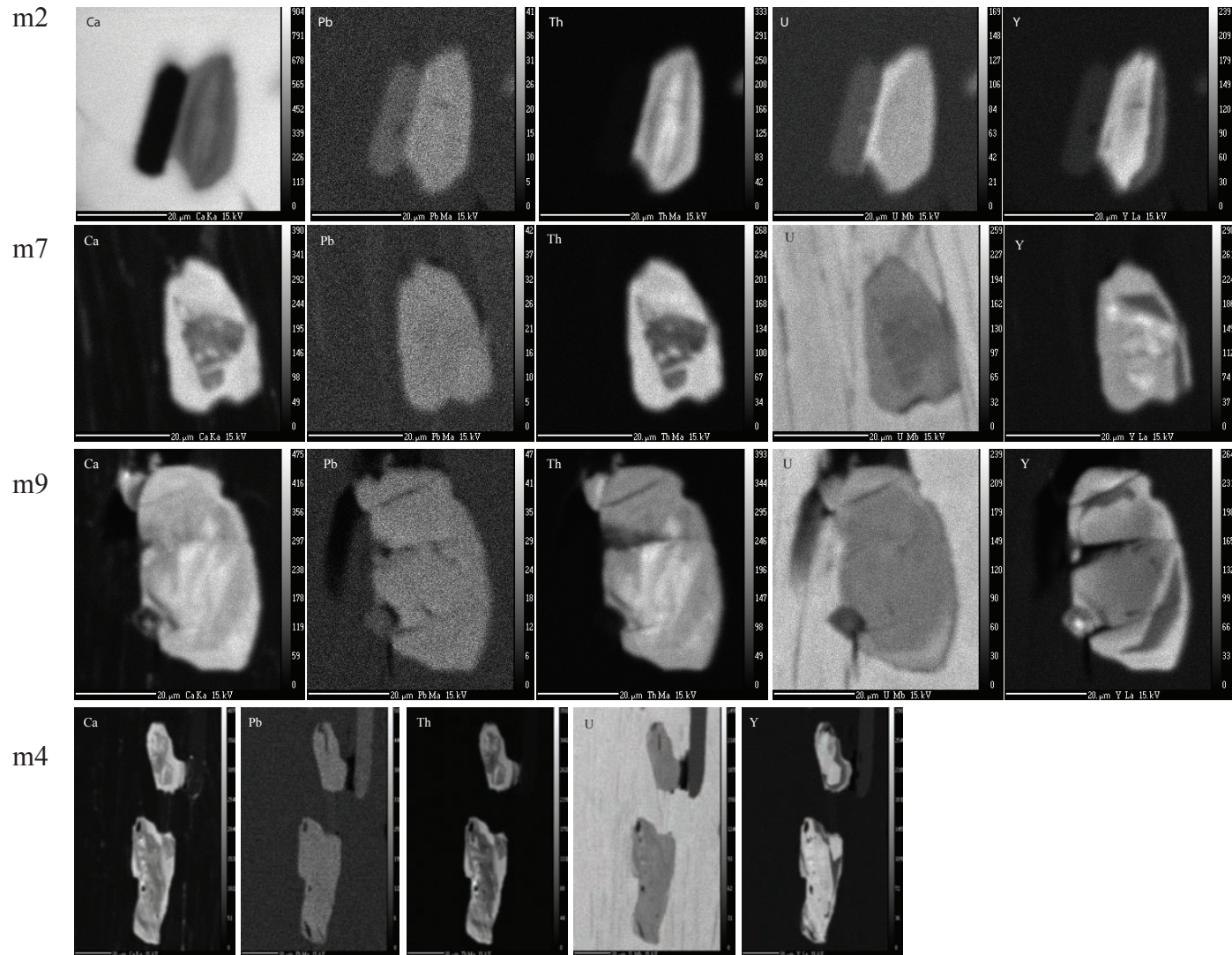


Figure 28. Compositional maps of monazite grains in sample 03 from the UMass microprobe.

defined. It is interesting to note that the Ca levels are elevated in the high Th domain and in the high U domain in m2 and m9. Although they yield similar ages, there is no correlation between the chemical compositions of m9 and m2 beyond the elevations in Ca. Figure 29 shows a histogram of all the ages for all domains analyzed.

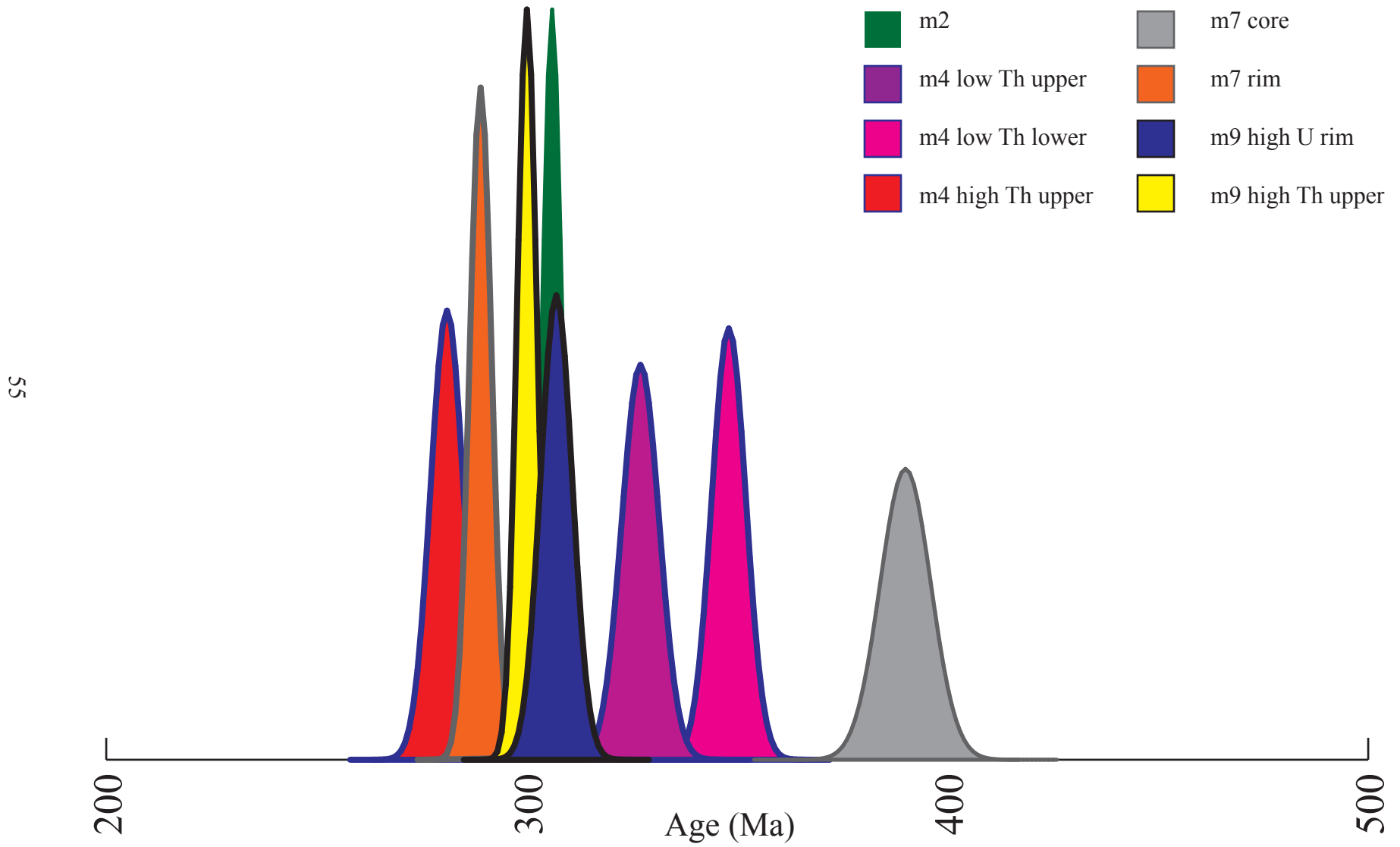


Figure 29. Histogram of monazite growth from sample 03.



## DISCUSSION

### **L'Espinouse**

The metamorphic grade is lower in L'Espinouse subdome than in the Rosis Syncline or Le Caroux subdome. This was anticipated in the field because the phyllitic rocks in L'Espinouse imply a lower grade of metamorphism than the schists and augen gneisses of the Rosis Syncline and Le Caroux. The phyllites are fine-grained and only show biotite-chlorite zone metamorphism as evidenced by their mineral assemblages (Table 1). The samples from L'Espinouse also lack garnet, staurolite, and aluminosilicates, the presence of which would indicate higher grades of metamorphism. In addition to the absence of these minerals, the abundance of chlorite suggests a lower grade, as chlorite is a dominant mineral in pelitic assemblages of lower pressures and temperatures (Spear, 1995). XRD analyses of two samples (32 and 33) show peaks congruent with clinochlorite. The biotite-tourmaline thermometer yields the same temperatures, within error, for L'Espinouse and the Rosis Syncline. However, the dominance of phyllites in L'Espinouse and schists in the Rosis Syncline suggests that the Rosis Syncline was subjected to higher temperatures than L'Espinouse. Sample 32 yielded a temperature of  $500 \pm 25$  °C from the tourmaline-biotite Fe-Mg exchange thermometer (Figure 22). This appears to be greater than what is expected for a chlorite-rich rock (Spear, 1995), but it may be that sample 32 is rich in chlorite as the result of retrograde metamorphism. In addition, the growth of Fe-rich carbonate growing in contact with a carbonate that falls along the dolomite-ankerite solid solution in Sample 15 from the Cours parking lot is evidence that this rock may have been reset at very low temperatures, as suggested by

Essene (1983). If this metamorphism did not affect the tourmaline and biotite, then the peak metamorphic temperatures may have been preserved.

### **Rosis Syncline**

From east to west, the rocks in the Rosis Syncline range from schists to metatexites. This suggests that the rocks in the syncline follow the overall trend in the eastern end of the Axial Zone of increasing metamorphic grade from east to west. Sample 27 is the westernmost sample containing muscovite and quartz that was collected from this region. The presence of muscovite places sample 27 downgrade from the muscovite-out isograd defined by the reaction



on the P-T grid (Figure 16). With a temperature of  $575 \pm 50$  °C, it is only possible to conclude that the pressure was above 2 kbars (Figure 16). It is difficult to place the muscovite-out isograd because sample 09 is the only rock with an assemblage of biotite + sillimanite + cordierite(?) and it was collected several kilometers west of sample 27. However, I have suggested its location between stations 27 and 25 on Figure 30. Sample 09 is a metatexite with ribbons of granite (partial melt). Fibrolite is present in the restite and it is possible that cordierite is also present. The assemblage here places the rock above 650 °C (Spear, 1995). Sample 09 lies in the core of L'Espinoise based on its high temperature and the presence of partial melts.

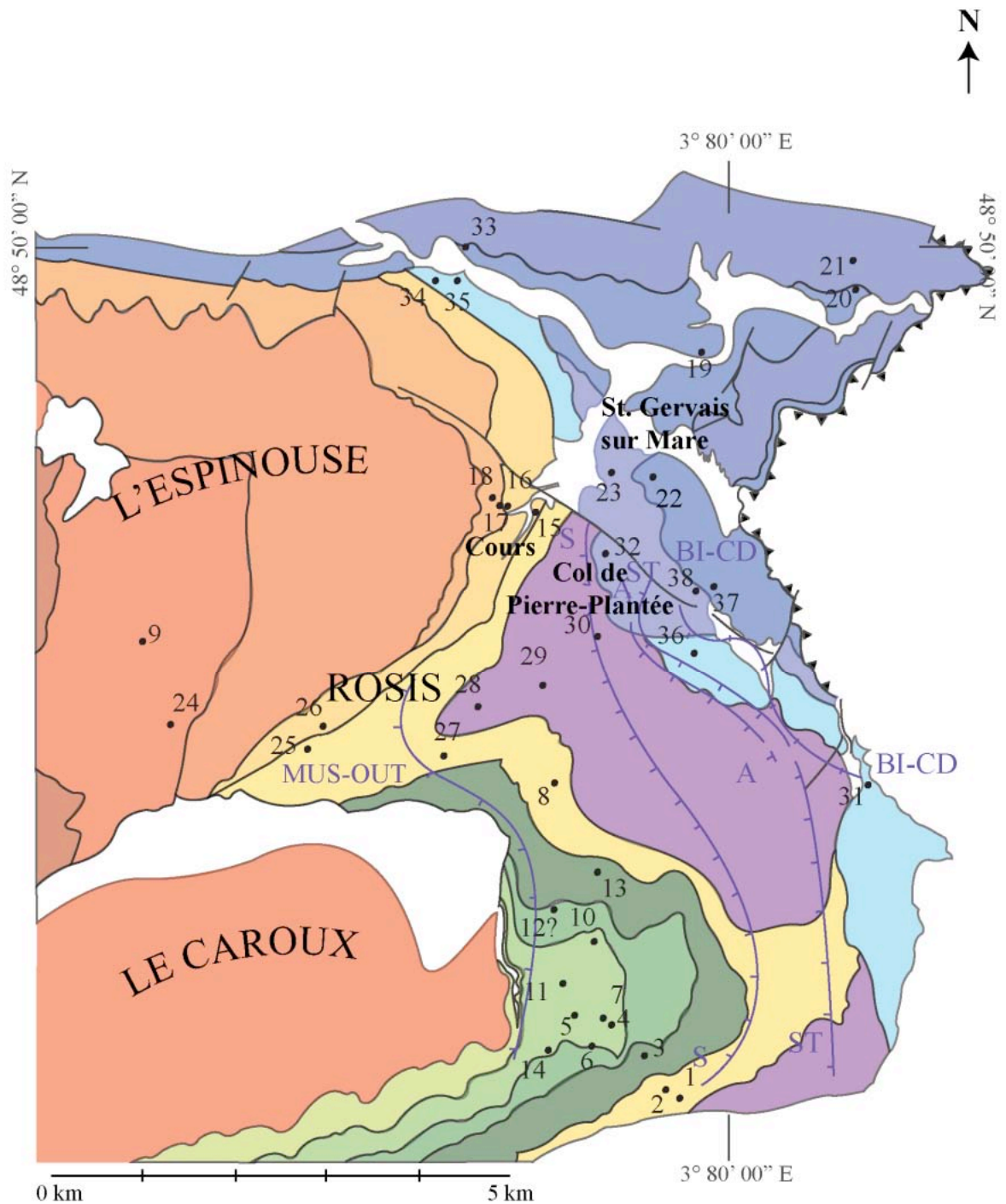


Figure 30. Geologic map of the eastern end of the Zone Axiale in the Montagne Noire Gneiss Dome, Montagne Noire, France with isograds after Thompson and Bard (1982) and suggested mus-out isograd. Mineral abbreviations: BI = biotite, CD = cordierite, ST = staurolite, A = andalusite, and S = sillimanite. Station locations are plotted and numbered.

## **Le Caroux**

A major assumption was made when interpreting the mineral assemblages in Le Caroux subdome. A bulk composition was calculated for sample 02 (Figure 31) and based on its low-Al bulk composition I have made interpretations of other samples in Le Caroux based on the assumption that they are also low-Al schists.

Overall, Le Caroux subdome experienced higher grades of metamorphism than L'Espinouse subdome. The mineral assemblages and geothermobarometry indicate peak temperatures at a minimum of 50 °C greater in Le Caroux than in L'Espinouse based on the samples of highest grade from each subdome. Within the metasedimentary envelope of Le Caroux, the mineral assemblages of the samples indicate progressively higher grades of metamorphism to the west. Pressures and temperatures obtained from four samples in Le Caroux using the garnet-biotite thermometer and the garnet-biotite-plagioclase-muscovite and garnet-biotite-plagioclase-quartz barometers are plotted in Figure 28 and their station locations are plotted in Figure 1.

Thompson and Bard (1982) drew a series of isograds across the eastern end of the Axial Zone based on a detailed transect across the Rosis Syncline. The isograds were extended south to Le Caroux subdome where they diverged “due to topographic relief” (Thompson and Bard, 1982). The first significant change in the mineral assemblages is the appearance of staurolite in sample 02. Based on the mineral assemblages of the rocks in Le Caroux, the staurolite-in isograd plots to the east of samples 02, 03, and 13. This is in agreement with the staurolite-in isograd drawn by Thompson and Bard. However, it is unclear whether sample 01 plots upgrade or downgrade from the staurolite-in isograd because it has neither the assemblage biotite + chlorite, which would place it downgrade,

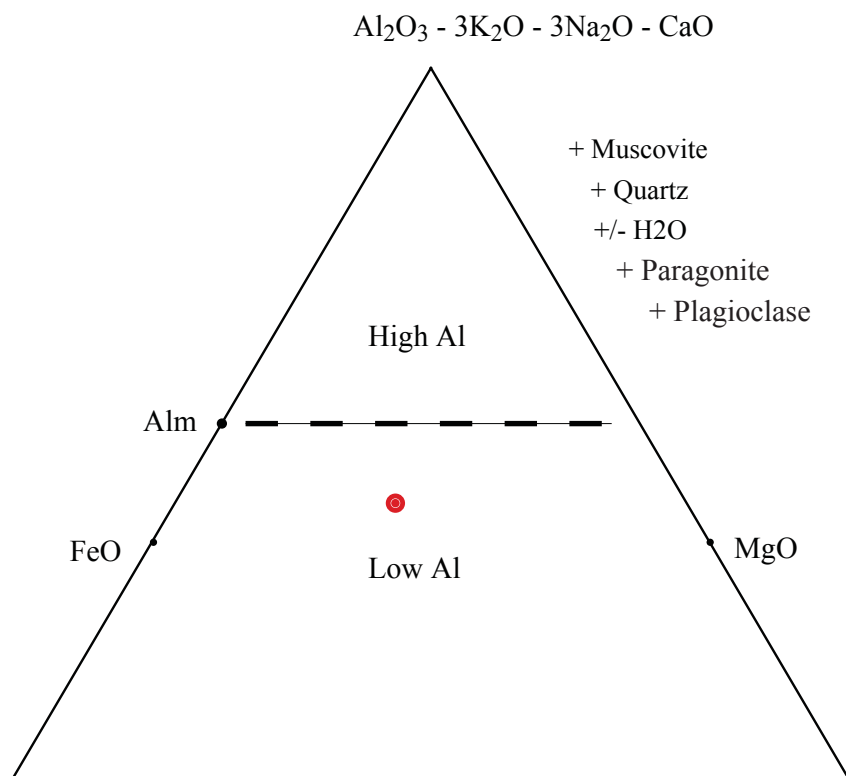
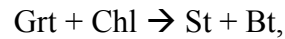


Figure 31. AFM diagram with bulk composition of sample 02 plotted in red. This is a low-Al metapelite. Alm = almandine.

nor the assemblage garnet + staurolite, which would place it upgrade. Based on this, I propose the drawing of the staurolite-in isograd, from the reaction



before station 02, but not necessarily after station 01 which is consistent with Thompson and Bard's staurolite-in isograd (Figure 3). Neither staurolite nor chlorite is present in sample 01, thus the rock does not have a bulk composition conducive for the determination of whether or not the chlorite-biotite tie-line has been broken at this location. The presence of staurolite in samples 02, 03, and 13 places them upgrade from the staurolite-in isograd, but on the P-T grid the pressures and temperatures calculated from the garnet-biotite thermometer and garnet-biotite-plagioclase-quartz and the garnet-biotite-plagioclase-quartz barometers plot downgrade from this isograd (Figure 32). This leads me to conclude that the Ps and Ts calculated from geothermometers for samples 02, 03 and 13 are not peak Ps and Ts, which would have to be at least 50 °C greater than those obtained using the garnet-biotite thermometer and the garnet-biotite-plagioclase-muscovite and garnet-biotite-plagioclase-quartz barometers.

It is plausible that the staurolite-out isograd defined by the reaction



may be placed in Le Caroux. Samples 13 and 03, located north and south of each other in the same map unit, both have mineral assemblages that include garnet and staurolite.

Staurolite is not present in any samples to the west of stations 03 and 13 (Table 1 and Figure 3). However, no garnet or aluminosilicate is present in samples west of 03 and 13 so it is not possible to definitively place the isograd. It is possible that none of the samples collected west of 03 and 13 have bulk compositions that would allow for the

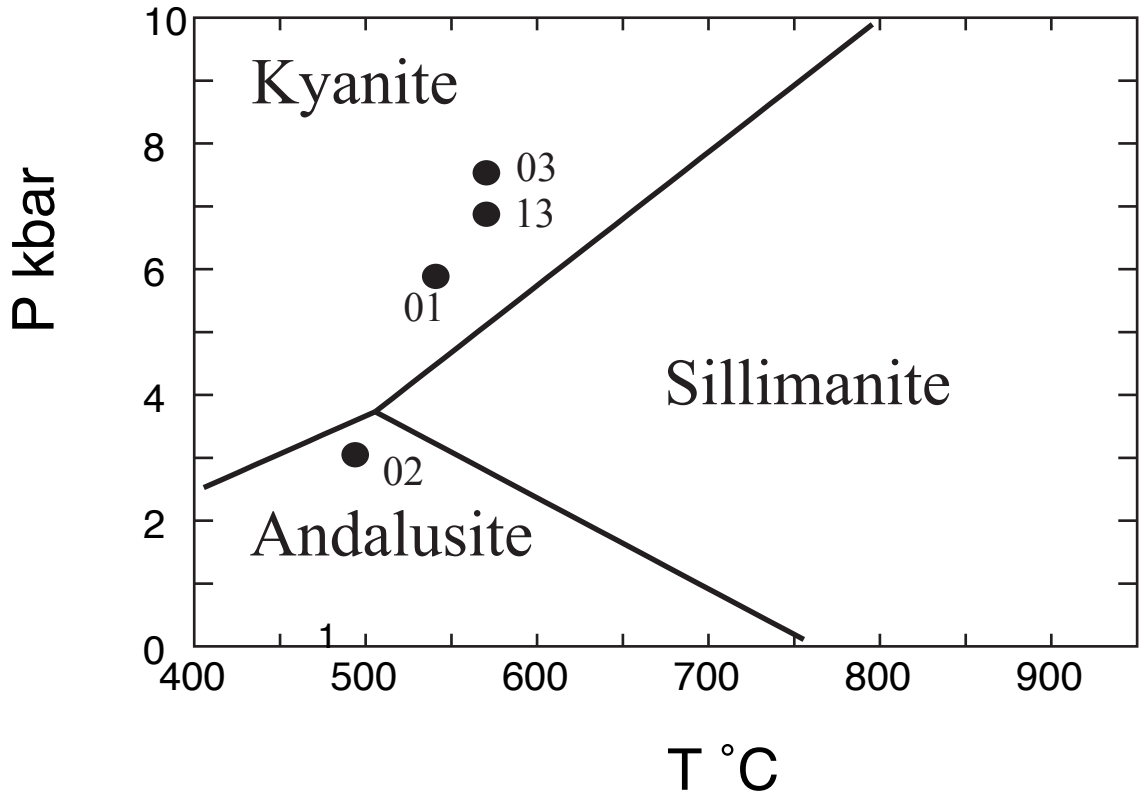
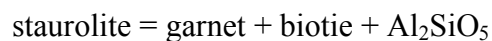


Figure 32. Graph of pressures and temperatures for samples 01, 02, 03, and 13 obtained using the program GTB (Kohn and Spear, 2001). Sample 13 plots in the kyanite zone even though its mineral assemblage garnet + biotite + staurolite + sillimanite places it between the staurolite isograds in the sillimanite zone.

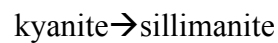
growth of these minerals. Thus, all that can be concluded is that if the staurolite-out reaction occurs, it is west of stations 03 and 13.

Thompson and Bard (1982) also drew the sillimanite isograd to the east of the samples collected in this study (Figure 3). Although it is possible that this isograd falls where they placed it, there is no evidence of sillimanite to the east of sample 13 which is to the west of the sillimanite isograd. Samples 01, 02, and 03 have assemblages that do not include sillimanite and their Ps and Ts plot in the kyanite zone (Figure 32). There is a discrepancy between the Ps and Ts yielded using GTB and the mineral assemblage of sample 13. Sample 13 has the assemblage garnet + staurolite + biotite + fibrolite, but plots in the kyanite zone, even with the 50 °C increase (Figure 32). This is a clear indication that the Ps and Ts obtained for sample 13 (and, therefore, for other samples) do not show the grade at which the rock equilibrated. The P and T yielded using GTB may express retrograde conditions. In this case the fibrolite would be relict and the rock may not have reequilibrated. This seems reasonable because the fibrolite is present in bands of muscovite and biotite and appears to be at the beginning stages of growth. Another possible explanation is that the garnet-biotite-plagioclase-muscovite barometer is not suited well for these rocks. It is unclear what the controls are on the applicability of the barometer (Ghent and Stout, 1981). There is also the issue of the assemblage garnet + staurolite + biotite + fibrolite: there are too many phases for the KFMASH system. There are two possible explanations for this: (1) we are seeing evidence of the staurolite-out reaction





in which staurolite breaks down and an aluminosilicate, in this case fibrolite, begins to grow, or (2) with the addition of components CaO and MnO, which are present in the garnet, comes the addition of another phase. If the former explanation were correct, then the staurolite isograd would fall along station 13 and the reaction



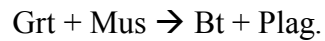
would fall to the east of station 13.

High-Mn garnet rims in sample 03 suggest garnet breakdown. When garnet is partially consumed the Mn is released into the matrix, but because Mn preferentially partitions into garnet, other minerals do not readily incorporate the Mn into their crystal lattices. Instead, back-diffusion of Mn into garnet creates high-Mn garnet rims (Kohn and Spear, 2000). Thus the presence of high-Mn rims on garnets in sample 03 suggests partial dissolution. This reaction is also reflected in the elevated concentration of Y in monazite. Like Mn, Y preferentially partitions into garnet, but during garnet breakdown the Y is released into the matrix and then incorporated into the crystal structure of growing monazites. The monazite domains in m2 and m9 in sample 03 that yielded ages of  $309 \pm 2.3$  Ma and  $307 \pm 3.8$  Ma, respectively, have high concentrations of Y relative to the surrounding domains (Figure 28). I propose that these monazite domains have higher concentrations of Y because they grew during the period of garnet breakdown. Therefore the reported ages represent the time of garnet breakdown in sample 03. Garnet is a reactant in the reaction that defines the first appearance of staurolite:



Because garnet is a reactant, it is partially consumed or dissolved. Thus the garnet dissolution corresponds to the growth of staurolite. Therefore, the monazite ages  $309 \pm$

2.3 Ma and  $307 \pm 3.8$  Ma may also represent the timing of the first appearance of staurolite (Figure 29). Another interpretation of the garnet breakdown is that garnet was involved in the decompression reaction



The relationship between growth of monazite domains and metamorphic processes is not as clear in sample 13. Monazites m2, m4, and m5 have high concentrations of Y relative to the older monazite domains, m7 and m3 and yield a weighted average of  $312 \pm 6$  Ma (Figures 25 and 26). However, within the individual monazite grains m2, m4, and m5, the concentration of Y is not divided into distinctly high and low Y domains so it is not possible to say that there are cores that correspond to older metamorphic events (Figure 25). Element maps for garnets were not gathered for sample 13 and no other evidence of garnet breakdown is apparent, yet the weighted average of clustered ages in sample 13 overlaps with the timing of garnet breakdown in sample 03 and may also be the timing of garnet breakdown in sample 13.

It is curious that there are peaks in samples 03 and 13 at  $326 \pm 4.4$  Ma and  $328 \pm 2.7$  Ma, respectively, that both coincide with the Vialais granite emplacement in L'Espinouse at  $327 \pm 5$  Ma (Matte et al., 1998). The exposure of the Vialais granite is too small and too far from the metasediments in Le Caroux and L'Espinouse to suggest regional contact metamorphism. It is possible that the exposure is not representative of the extent of the intrusion and future work may show a relationship between the monazite growth in the metasediments and the Vialais granite emplacement.

Monazite growth also occurred at  $347 \pm 4.1$  Ma and  $352 \pm 4$  Ma in samples 03 and 13, respectively. Although there is only one peak for each of these dates in each

sample, they are both within the error range of the major HT-LP regional deformation that took place in the Albigeois, north of the Axial Zone. It is plausible that the regional metamorphism dated in the north affected the rocks in the Axial Zone and that monazite growth is a record of this earlier metamorphism. The earliest peak in sample 03 dates at  $388 \pm 6$  Ma. This date does not correlate to any intrusions or metamorphic events discussed in the literature.

Le Caroux underwent multiple deformational events or pulses. The most compelling evidence for this is provided by the preserved cleavages in samples 03 and 13 (Figures 14 and 15). In sample 13, cleavages S1 and S3 are orthogonal to S2 in the plane parallel to lineation and perpendicular to the most recent foliation (Figure 15). This clearly indicates that at least three deformational pulses or events occurred during the formation of this schist. The two cleavages, S2, and S3, in sample 03 are also orthogonal to each other in the plane parallel to lineation and perpendicular to the most recent foliation (Figure 14). S2 and S3 in sample 03 have the same orientations as S2 and S3 in 13. It is possible that the corresponding cleavages between samples 03 and 13 represent the same cleavages and thus the same deformation pulses or events. These cleavages represent two distinct deformational pulses or events that were pervasive in Le Caroux. S<sub>1</sub> may be the bedding plane or it may represent the first cleavage. S<sub>2</sub> is orthogonal to S<sub>1</sub> and is consistent with shortening occurring within the dome. This shortening may have led to build-up followed by extensional collapse and shearing as evidenced by S<sub>3</sub>, which is parallel to S<sub>1</sub> and orthogonal to S<sub>2</sub>. Bell, Rubenach, and Fleming (1986) first proposed shortening followed by shearing (gravitational collapse) as a mechanism for the explanation of the succession of orthogonal cleavages. This also presents another

explanation for dissolution of garnet in sample 03. Dissolution of garnet occurs in shear zones and zones of shortening and folding are conducive to garnet nucleation and continued porphyroblastic growth (Bell et al., 1986). If shortening followed shearing, then the location would be ideal for dissolution of garnet followed by staurolite growth and renewed garnet growth in sample 03. In this series of events  $S_3$  represents the last gravitational collapse recorded in these rocks.

There is a fault that trends NW-SE that truncates the isograds that were first proposed by Thompson and Bard (1982) and confirmed by this study. This truncation separates the chlorite-biotite grade rocks to the north from the amphibolite-grade rocks to the south. There is a clear progression of increasing grade of metamorphism from east to west in Le Caroux and in the Rosis Syncline. However, the rocks to the north of the NW-SE trending fault do not provide evidence that would suggest that they underwent the same metamorphism as the rocks in the south. I propose that the fault postdates the metamorphism that produced the series of isograds in Le Caroux and in the Rosis Syncline and that the low-grade metamorphism observed in the northern rocks did not result from the same metamorphic events that caused the reaction sequence in the southern rocks.

## CONCLUSIONS

L'Espinouse saw a lower peak metamorphic grade than Le Caroux and the Rosis Syncline. It appears that the rocks in L'Espinouse only reached the biotite-chlorite zone of metamorphism. Based on thermobarometry, the Rosis Syncline increases in metamorphic grade from east to west, toward the core of the dome. The Rosis Syncline experienced slightly higher temperatures than L'Espinouse, reaching at least  $575 \pm 50$  °C in the metasedimentary envelope. In the core of the Montagne Noire Gneiss Dome the metatexites reached temperatures at a minimum of  $650 \pm 50$  °C.

Like the Rosis Syncline, the metamorphic grade increases from east to west toward the core in Le Caroux. However, the rocks from Le Caroux tell a more interesting story. The metasedimentary envelope reached temperatures of at least 625 °C.

Unfortunately, the bulk composition of these low-Al metapelites does not allow us to easily constrain the metamorphic history using mineral assemblages alone. When the  $P_s$  and  $T_s$  determined from the mineral assemblages are combined with  $P_s$  and  $T_s$  from thermobarometric programs, it becomes clear that peak metamorphic  $P_s$  and  $T_s$  have not been preserved in the chemical compositions. Therefore, the thermobarometry programs are yielding  $P_s$  and  $T_s$  of retrograde metamorphism.

It is possible that at least two events of gravitational collapse (shearing) in the metasedimentary envelope sandwich a shortening event. During one of the shearing events garnet dissolution was recorded in the growth of high Y domains in monazite at around 310 Ma. A NW-SE trending fault separates the biotite-chlorite grade phyllitic rocks to the north from the amphibolite grade schists to the south. This fault postdates the metamorphic event(s) that resulted in a series of reactions in the southern rocks.

## REFERENCES

- Aerden, D.G.A.M., 1998, Tectonic evolution of the Montagne Noire and a possible orogenic model for syncollisional exhumation of deep rocks, Variscan belt, France: *Tectonics*, v.17, p. 62-79.
- Bard, J.P., Rabeloson, R., 1973, Métamorphisme plurifacial de variation du degré géothermique Durant la tectogenèse polyphasée hercynienne dans la partie orientale de la zone axiale de la Montagne Noire (Massif du Caroux, Sud du Massif Central français): *Bulletin de la Societe Geologique de France*, v. 7, issues 5-6, p. 579-586.
- Bell, T.H., and Rubenach, M.J., 1986, Prophyroblast nucleation, growth and dissolution in regional metamorphic rocks as a function of deformation partitioning during foliation development: *Journal of Metamorphic Geology*, v. 4, Issue 1, p. 37-67.
- Cocherie, A., Baudin, T., Autran, A., Guerrot, C., Fanning, C.M., and Laumonier, B., 2005, U-Pb zircon (ID-TIMS and SHRIMP) evidence for the early ordovician intrusion of metagranites in the late Proterozoic Canaveilles Group of the Pyrenees and the Montagne Noire (France): *Bulletin de la Societe Geologique de France*, v. 176, Issue 3, p. 269-282.
- Ducrot, J., Lancelot, J.R., Reille, J.L., 1979, Datation en Montagne Noire d'un témoin d'une phase majeure d'amincissement crustal caractéristique de l'Europe prevarisque: *Bulletin de la Societe Geologique de France*, v. 21, issue 4, p. 501-505.
- Echtler, H. and Malavieille, J., 1990, Extensional tectonics, basement uplift and Stephano-Permian collapse basin in a late Variscan metamorphic core complex (Montagne Noire, Southern Massif Central): *Tectonophysics*, v. 177, p. 125-138.
- Essene, E.J., 1983, Solid solutions and solvi among metamorphic carbonates with applications to geologic thermobarometry, *in Reviews in Mineralogy*, v. 11, p. 77-96.
- Franke, W., Doublier, M.P., Stein, E., Klama, K.O., Dörr, W., Wiederer, U., and Königshof, P., 2002, Exhumation of LP rocks in the Montagne Noire: New facts and models *in Abstract volume, 19ème Réunion des Sciences de la Terre* (Nantes), p. 120.
- Ghent, D.E. and Stout, M.Z., 1981, Geobarometry and geothermometry of plagioclase-biotite-garnet-muscovite assemblages: *Contributions to Mineralogy and Petrology*, v. 76, p. 92-97.
- GTB February 2001 version, Matthew J. Kohn, Dept. of Geological Sciences, University of South Carolina, Columbia, SC 29208 and Frank Spear, Dept. of Earth and Environmental Sciences, Rensselaer Polytechnic Institute, Troy, NY 12180.
- Kohn, M.J., and Spear, F., 2000, Retrograde net transfer reaction insurance for pressure-temperature estimates: *Geology Boulder*, v. 28, Issue 12, p. 1127-1130.
- Lescuyer and Cocherie, 1992, Datation sur monozircons des metadacites de Series; arguments pour un age proterozoique terminal des 'schistes X' de la Montagne Noire (Massif central francais): *Comptes Rendus de l'Academie des Sciences*, v. 314, Issue 10, p. 1071-1077.

- Matte, P., 1986, Tectonics and plate tectonics model for the Variscan Belt of Europe: *Tectonophysics*, v. 126, Issue 2-4, p. 329-374.
- Matte, P., 1991, Accretionary history and crustal evolution of the Variscan Belt in Western Europe: *Tectonophysics*, v. 196, Issue 3-4, p. 309-337.
- Matte, P., Lancelot, J., Mattauer, M., 1998, La zone axiale hercynienne de la Montagne Noire n'est pas un 'metamorphic core complex' extensive mais un anticlinal post-nappe a Coeur anatectique: *Geodinamica Acta*, v. 11, Issue 1, p. 13-22.
- Matte, P., 2001, The Variscan collage and orogeny (480-290 Ma) and the tectonic definition of the Armorica microplate: a review: *Terra Nova*, v. 13, p. 122-128.
- Matte, P., 2006, Variscan thrust nappes, detachments and strike-slip faults in the Massif Central Français: the interpretation of the lineations:
- Menning, M., Weyer, D., Drozdowski, G., Van Amerom, H.W.J., and Wendt, I., 2000, A Carboniferous Time Scale 2000: Discussion and Use of Geological Parameters as Time Indicators from Central and Western Europe: *Geologisches Jahrbuch Hannover*, v. 156, p. 3-44.
- Nesse, W.D., 2000, *Introduction to mineralogy*: New York, Oxford University Press, 442 p.
- Ourzik, A., Debat, P., and Mercier, A., 1991, Évolution métamorphique de la partie N et NE de la zone axiale de la Montagne noire (Sud du Massif Central, France): *Comptes rendus de l'Académie des sciences*, v. 313, p. 1547-1553.
- Soula, J.C., Debat, P., Brusset, S., Bressière, G., Christophoul, J. D., 2001, Thrust-related, diapiric, and extensional doming in a frontal orogenic wedge: example of the Montagne Noire, Southern French Hercynian Belt: *Journal of Structural Geology*, v. 23, p. 1677-1699.
- Spear, F.S., 1995, *Metamorphic phase equilibria and pressure-temperature-time paths*: Washington, Mineralogical Society of America, 799 p.
- Thompson, P.H., and Bard, J.P., 1982, Isograds and mineral assemblages in the eastern axial zone, Montagne Noire (France): implications for temperature gradients and P-T history: *Canadian Journal of Earth Sciences*, v. 19, p. 129-143.
- Van den Driessche, J., and Brun, J.P., 1992, Tectonic evolution of the Montagne Noire (french Massif Central): a model of extensional gneiss dome: *Geodinamica Acta*, v. 5, p. 85-99.
- Van der Pluijm, B.A., Marshak, S., 2004, *Earth Structure*: New York, W.W. Norton & Company, 656 p.
- Vanderhaeghe, O., 2004, Structural development of the Naxos migmatite dome, in Whitney, D.L., Teyssier, C., and Siddoway, C.S., eds., *Gneiss domes in orogeny*: Boulder, Colorado, Geological Society of America Special Paper 380, p.15-33.
- Williams, M.L., Jercinovic, M.J., Goncalves, P., Mahan, K., Format and philosophy for collecting, compiling, and reporting microprobe monazite ages: *Chemical Geology*, v. 225, Issue 1-2, p. 1-15.
- Winter, J.D., 2001, *An introduction to igneous and metamorphic petrology*: Upper Saddle River, NJ, Prentice Hall, 697 p.
- Whitney, D.L., Teyssier, C., and Vanderhaeghe, O., 2004, Gneiss domes and crustal flow, in Whitney, D.L., Teyssier, C., and Siddoway, C.S., eds., *Gneiss domes in*

orogeny: Boulder, Colorado, Geological Society of America Special Paper 380, p.15-33.

Yin, A., 2004, Gneiss domes and gneiss dome systems, *in* Whitney, D.L., Teysier, C., and Siddoway, C.S., eds., Gneiss domes in orogeny: Boulder, Colorado, Geological Society of America Special Paper 380, p. 1-14.



APPENDIX A: Geothermobarometry spreadsheets for Kohn and Spear's GTB



**Text file used for Kohn and Spear's Program Geothermobarometry for 06MN02a**

13

Sample	Point	Oxnorm	Wt%tot	CNa	CMg	CAI	CSi	CK	CCa	CTi	CMn	CFe2+
GAR1C1	1	12	99.74	0.00	0.25	2.04	3.00	0.00	0.18	0.00	0.46	2.04
GAR1R1	2	12	95.66	0.00	0.32	2.00	3.01	0.00	0.11	0.00	0.33	2.24
GAR1R2	3	12	100.45	0.00	0.31	2.04	3.01	0.00	0.11	0.00	0.32	2.19
GAR1R3	4	12	100.10	0.00	0.33	2.05	3.01	0.00	0.12	0.00	0.31	2.15
GAR2R1	5	12	100.67	0.00	0.33	2.05	2.99	0.00	0.12	0.00	0.32	2.16
GAR2R1	6	12	100.43	0.00	0.32	2.07	3.00	0.00	0.11	0.00	0.31	2.14
GAR2R2	7	12	99.68	0.00	0.32	2.04	3.00	0.00	0.11	0.00	0.31	2.20
GAR2R3	8	12	98.48	0.00	0.31	2.02	3.01	0.00	0.11	0.00	0.32	2.19
GAR3R1	9	12	101.52	0.00	0.32	2.05	3.02	0.00	0.12	0.00	0.30	2.15
GAR3R2	10	12	100.87	0.00	0.32	2.05	2.99	0.00	0.11	0.00	0.31	2.19
GAR3R4	11	12	96.17	0.00	0.30	2.03	2.97	0.00	0.13	0.00	0.32	2.26
GAR3R5	12	12	99.36	0.00	0.33	2.03	2.98	0.00	0.13	0.00	0.34	2.20
GAR4C1	13	12	101.61	0.00	0.26	2.07	3.04	0.00	0.15	0.00	0.43	1.98
GAR4R1	14	12	98.61	0.00	0.29	2.02	3.01	0.00	0.13	0.00	0.34	2.19
GAR4_2	15	12	98.41	0.00	0.30	2.03	3.01	0.00	0.12	0.00	0.34	2.18
BIO1	16	11	94.45	0.05	1.15	1.86	2.70	0.87	0.00	0.01	0.00	1.19
BIO2	17	11	93.88	0.06	1.08	1.83	2.73	0.89	0.00	0.00	0.00	1.23
BIO3	18	11	99.61	0.07	1.15	1.84	2.76	0.82	0.00	0.00	0.00	1.12
BIO4	19	11	94.43	0.05	1.13	1.85	2.74	0.87	0.00	0.00	0.00	1.16
BIO5	20	11	96.91	0.06	1.13	1.83	2.70	0.88	0.00	0.00	0.07	1.12
BIO6	21	11	94.75	0.08	1.11	1.80	2.68	0.88	-0.01	0.09	0.00	1.18
BIO7	22	11	86.12	-0.02	1.12	1.87	2.85	0.00	-0.01	0.10	0.00	1.19
FSP1	23	8	94.93	0.12	0.05	2.05	2.25	0.55	0.00	0.00	0.00	0.04
FSP2	24	8	93.96	0.13	0.00	2.11	2.25	0.53	0.00	0.00	0.00	0.00
FSP3	25	8	122.32	0.84	0.00	1.25	2.75	0.03	0.19	0.00	0.00	0.00
FSP4	26	8	102.25	0.77	0.00	1.27	2.75	0.02	0.22	0.00	0.00	0.00
FSP5	27	8	93.01	0.13	0.04	2.13	2.22	0.51	0.00	0.00	0.00	0.00
FSP6	28	8	92.20	0.69	0.00	1.24	2.81	0.20	0.08	0.00	0.00	0.00
FSP7	29	8	106.16	1.43	0.00	1.41	4.08	0.01	0.00	0.00	0.00	0.00
MUS1	30	11	92.88	0.16	0.00	2.89	3.07	0.81	0.00	0.02	0.00	0.00

MUS2	31	11	93.26	0.21	0.00	2.95	3.01	0.76	0.01	0.03	0.00	0.00
MUS3	32	11	91.01	0.18	0.00	2.94	3.06	0.78	-0.01	0.00	0.00	0.00
MUS4	33	11	93.62	0.20	0.00	2.89	3.10	0.78	-0.01	0.00	0.00	0.00
MUS5	34	11	101.09	0.23	0.00	2.90	3.10	0.70	0.00	0.00	0.00	0.00
ST2	35	47	98.03	0.17	0.63	18.42	7.79	0.00	0.00	0.10	0.00	2.87
ST3	36	47	98.54	0.13	0.82	18.30	7.72	0.00	0.00	0.12	0.00	2.98
CHL1	37		90.88	0.00	7.36	10.03	8.81	0.00	0.00	0.00	0.00	6.98
CHL2	38		88.90	0.00	7.65	10.07	8.69	0.00	0.00	0.00	0.00	6.86
TUR1	39	15	88.45	0.42	1.00	3.80	3.65	0.00	0.06	0.04	0.00	0.64
TUR2	40	15	89.22	0.34	0.91	4.00	3.61	0.00	0.07	0.05	0.00	0.53

**Text file used for Kohn and Spear's Program Geothermobarometry for 06MN03**

13

Sample	Point	Oxnorm	Wt%tot	CNa	CMg	CAI	CSi	CK	CCa	CTi	CMn	CFe2+
UNK1	1	12	86.90	0.00	0.00	2.01	3.00	0.00	0.23	0.00	0.00	2.75
GAR1C	2	12	98.22	0.00	0.19	2.02	2.99	0.00	0.40	0.00	0.27	2.14
GAR1C	3	12	99.17	0.00	0.18	2.03	3.00	0.00	0.37	0.00	0.29	2.12
GAR1R	4	12	99.60	0.00	0.22	2.04	2.96	0.00	0.34	0.00	0.19	2.25
GAR1R2	5	12	106.31	0.00	0.37	2.06	3.10	0.00	0.15	0.00	0.14	2.04
GAR1R3	6	12	98.86	0.00	0.32	2.05	3.00	0.00	0.20	0.00	0.13	2.28
GAR2C	7	12	100.56	0.00	0.14	2.01	3.01	0.00	0.52	0.00	0.46	1.85
GAR2C1	8	12	101.46	0.00	0.14	2.01	2.99	0.00	0.51	0.00	0.47	1.86
GAR2R1	9	12	101.45	0.00	0.18	2.00	3.01	0.00	0.41	0.00	0.21	2.18
GAR2R2	10	12	100.97	0.00	0.32	2.04	2.99	0.00	0.18	0.00	0.07	2.39
GAR2R3	11	12	100.54	0.00	0.21	2.01	3.01	0.00	0.37	0.00	0.17	2.22
GAR2R4	12	12	101.39	0.00	0.16	2.03	3.01	0.00	0.45	0.00	0.36	1.97
GAR2R5	13	12	100.69	0.00	0.29	2.04	2.99	0.00	0.21	0.00	0.12	2.33
GAR2R6	14	12	100.76	0.00	0.21	2.00	3.01	0.00	0.35	0.00	0.16	2.24
GAR2R7	15	12	97.38	0.00	0.31	2.02	3.00	0.00	0.22	0.00	0.20	2.23
GAR2R8	16	12	100.58	0.00	0.32	2.06	3.00	0.00	0.18	0.00	0.14	2.28
GAR3R1	17	12	100.80	0.00	0.31	2.02	2.98	0.00	0.19	0.00	0.04	2.46
GAR3C1	18	12	101.47	0.00	0.27	2.03	2.99	0.00	0.19	0.00	0.10	2.41
GAR3C2	19	12	100.24	0.00	0.28	2.03	3.00	0.00	0.18	0.00	0.09	2.41
GAR3R2	20	12	100.02	0.00	0.30	2.04	3.02	0.00	0.17	0.00	0.05	2.39
GAR3R3	21	12	100.41	0.00	0.31	2.01	3.03	0.00	0.17	0.00	0.23	2.21
GAR4R1	22	12	95.16	0.00	0.29	1.95	2.98	0.00	0.19	0.00	0.06	2.58
GAR4R2	23	12	98.11	0.00	0.34	2.02	3.01	0.00	0.16	0.00	0.00	2.46
BIO1	24	11	95.91	0.00	1.12	1.83	2.78	0.83	0.00	0.00	0.01	1.16
BIO2	25	11	94.92	0.00	1.08	1.86	2.78	0.85	0.00	0.00	0.00	1.15
BIO3	26	11	93.21	0.00	1.12	1.88	2.73	0.83	0.00	0.00	0.01	1.18
BIO3a	27	11	94.41	0.09	1.12	1.80	2.68	0.82	0.01	0.08	0.00	1.19
BIO4	28	11	95.54	0.09	1.09	1.83	2.69	0.81	0.00	0.09	0.00	1.15
BIO5	29	11	88.71	0.11	1.06	1.83	2.68	0.83	0.00	0.07	0.00	1.24
BIO6	30	11	90.97	0.09	1.08	1.84	2.68	0.80	0.00	0.07	0.00	1.20

BIO7	31	11	99.11	0.10	1.13	1.83	2.70	0.75	0.02	0.07	0.00	1.16
BIO8	32	11	98.24	0.09	1.11	1.82	2.71	0.73	0.02	0.08	0.00	1.16
BIO9	33	11	84.84	0.07	1.04	1.76	2.64	0.84	0.02	0.10	0.00	1.37
BIO10	34	11	95.74	0.12	1.11	1.80	2.70	0.78	0.01	0.08	0.00	1.17
BIO11	35	11	95.16	0.10	1.10	1.79	2.71	0.78	0.01	0.09	1.17	1.17
FSP1	36	8	98.41	0.90	0.00	1.14	2.86	0.01	0.11	0.00	0.00	0.00
FSP2	37	8	99.66	0.77	0.00	1.14	2.90	0.01	0.10	0.00	0.00	0.00
FSP3	38	8	100.77	1.29	0.00	1.75	4.26	0.00	0.20	0.00	0.00	0.00
FSP4	39	8	96.45	1.27	0.00	1.75	4.26	0.00	0.23	0.00	0.00	0.00
FSP5	40	8	99.26	0.86	0.00	1.15	2.87	0.00	0.11	0.00	0.00	0.00
MUS1	41	11	93.77	0.19	0.00	2.92	3.06	0.71	0.00	0.02	0.00	0.00
MUS2	42	11	94.96	0.18	0.00	2.93	3.07	0.66	0.01	0.03	0.00	0.00
MUS3	43	11	89.40	0.18	0.00	2.95	2.95	3.06	0.73	0.01	0.00	0.00
MUS4	44	11	95.61	0.22	0.00	2.94	3.06	0.71	0.00	0.00	0.00	0.00

**Text file used for Kohn and Spear's Program Geothermobarometry for 06MN12**

13

Sample	Point	Oxnorm	Wt%tot	CNa	CMg	CAI	CSi	CK	CCa	CTi	CMn	CFe2+
TUR1C1	1	15	86.86	0.46	0.93	3.96	3.63	0.08	0.08	0.00	0.00	0.57
TUR1C2	2	15	85.16	0.47	1.02	3.60	3.75	0.07	0.07	0.00	0.00	0.76
TUR1C3	3	15	85.41	0.40	1.04	3.84	3.66	0.10	0.10	0.00	0.00	0.57
BIO1	4	11	95.63	0.00	0.96	1.75	2.74	0.87	0.16	0.16	0.00	1.18
BIO2	5	11	96.73	0.00	0.99	1.77	2.71	0.86	0.17	0.17	0.00	1.16

**Text file used for Kohn and Spear's Program Geothermobarometry for 06MN13**

13

Sample	Point	Oxnorm	Wt%tot	CNa	CMg	CAI	CSi	CK	CCa	CTi	CMn	CFe2+
GAR1_R1	1	12	98.11	0.00	0.31	2.02	3.00	0.00	0.27	0.00	0.36	2.04
GAR1_R2	2	12	98.51	0.00	0.33	2.02	3.00	0.00	0.27	0.00	0.36	2.02
GAR1C1	3	12	98.21	0.00	0.25	2.00	3.02	0.00	0.41	0.00	0.46	1.84
GAR2R1	4	12	99.51	0.00	0.34	2.04	3.00	0.00	0.16	0.00	0.42	2.02
GAR2C1	5	12	97.88	0.00	0.25	2.02	2.99	0.00	0.39	0.00	0.40	1.95
GAR2R2	6	12	91.34	0.00	0.28	2.01	2.91	0.00	0.42	0.00	0.47	1.99
GAR4C1	7	12	99.86	0.00	0.23	2.03	2.99	0.00	0.47	0.00	0.47	1.81
GAR4R1	8	12	100.37	0.00	0.34	2.05	2.99	0.00	0.22	0.00	0.41	1.96
GAR6C1	9	12	97.50	0.00	0.30	1.99	3.01	0.00	0.17	0.00	0.42	2.12
GAR6R1	10	12	103.55	0.00	0.34	2.07	3.06	0.00	0.20	0.00	0.42	1.82
GAR6R2	11	12	0.00	0.00	0.00	0.00	0.00	0.00	0.00	0.00	0.00	0.00
GAR5R1	12	12	99.79	0.00	0.35	2.03	3.02	0.00	0.23	0.00	0.36	1.98
GAR8C1	13	12	98.34	0.00	0.29	2.03	3.02	0.00	0.31	0.00	0.43	1.89
GAR8R1	14	12	97.06	0.00	0.33	2.03	2.99	0.00	0.30	0.00	0.35	2.00
GAR8R2	15	12	98.12	0.00	0.31	2.04	3.00	0.00	0.23	0.00	0.43	1.96
GAR8R3	16	12	112.44	0.00	0.38	2.12	3.08	0.00	0.19	0.00	0.35	1.74
BIO1	17	11	93.17	0.07	1.15	1.80	2.70	0.86	0.00	0.08	0.00	0.00
BIO2	18	11	95.70	0.04	1.16	1.80	2.71	0.84	-0.01	0.10	0.00	1.11
BIO3	19	11	93.39	0.04	1.06	1.65	2.48	0.77	0.00	0.00	0.00	1.10
BIO4	20	11	92.27	0.08	1.11	1.85	2.77	0.83	0.00	0.00	0.00	1.12
BIO5	21	11	93.56	0.07	1.14	1.85	2.75	0.83	0.01	0.00	0.00	1.12
BIO6	22	11	0.00	0.00	0.00	0.00	0.00	0.00	0.00	0.00	0.00	0.00
BIO7	23	11	96.50	0.10	1.13	1.88	2.63	0.82	0.08	0.00	0.00	1.16
BIO8	24	11	93.46	0.09	1.17	1.80	2.69	0.85	0.01	0.08	0.00	1.11
BIO9	25	11	96.83	0.08	1.16	1.80	2.72	0.82	0.01	0.08	0.00	1.08
BIO10	26	11	91.86	0.10	1.10	1.85	2.65	0.83	0.00	0.11	0.00	1.13
FSP1	27	8	101.17	0.77	0.00	1.25	2.76	0.01	0.21	0.00	0.00	0.09
FSP2	28	8	100.96	0.74	0.00	1.25	2.75	0.00	0.24	0.00	0.00	0.00
FSP2?	29	8	103.78	0.72	0.00	1.24	2.78	0.02	0.22	0.00	0.00	0.00
FSP3	30	8	100.92	0.73	0.00	1.25	2.76	0.02	0.23	0.00	0.00	0.00



FSP4	31	8	101.38	0.74	0.00	1.25	2.77	0.00	0.22	0.00	0.00	0.00
FSP5	32	8	100.21	0.77	0.00	1.24	2.76	0.00	0.23	0.00	0.00	0.00
FSP6	33	8	98.51	0.76	0.00	1.24	2.76	0.00	0.23	0.00	0.00	0.00
FSP7	34	8	97.56	0.16	0.00	1.10	2.96	0.00	0.71	0.00	0.00	0.00
FSP8	35	8	100.89	0.77	0.00	1.26	2.74	0.01	0.24	0.00	0.00	0.00
FSP9	36	8	100.48	0.66	0.00	1.24	2.78	0.00	0.24	0.00	0.00	0.00
FSP10	37	8	0.00	0.00	0.00	0.00	0.00	0.00	0.00	0.00	0.00	0.00
MUS1	38	11	87.24	0.00	0.10	2.75	3.12	0.92	0.00	0.00	0.00	0.00
MUS2	39	11	101.49	0.00	0.00	1.42	4.10	1.36	0.00	0.00	0.00	0.08
MUS3	40	11	97.18	0.00	0.00	1.47	4.12	1.00	0.05	0.00	0.00	0.00
MUS4	41	11	93.53	0.07	0.00	2.97	3.16	0.35	0.00	0.00	0.00	0.00
IL1	42	3	92.87	0.00	0.00	0.00	0.00	0.00	0.00	1.05	0.00	0.90
UNK1	43	12	79.80	0.00	0.79	2.39	2.25	0.00	0.00	0.00	0.00	3.13

**Text file used for Kohn and Spear's Program Geothermobarometry for 06MN27**

13

Sample	Point	Oxnorm	Wt%tot	CNa	CMg	CAI	CSi	CK	CCa	CTi	CMn	CFe2+
TUR1	1	15	86.20	0.32	0.76	3.12	2.93	0.00	0.05	0.03	0.00	0.43
TUR2	2	15	88.12	0.40	0.98	4.00	3.61	0.00	0.04	0.03	0.00	0.49
TUR3	4	15	86.53	0.40	0.98	3.98	3.58	0.00	0.08	0.05	0.00	0.49
BIO1	5	11	97.52	0.09	1.06	1.81	2.67	0.86	0.00	0.14	0.00	1.13
BIO2	6	11	99.07	0.06	1.10	1.83	2.69	0.81	0.00	0.13	0.00	1.09
BIO3	7	11	93.32	0.08	1.00	1.82	2.68	0.85	0.00	0.15	0.00	1.14
FSP1	8	8	98.92	0.83	0.00	1.20	2.80	0.00	0.18	0.00	0.00	0.00

**Text file used for Kohn and Spear's Program Geothermobarometry for 06MN32**

13

Sample	Point	Oxnorm	Wt%tot	CNa	CMg	CAI	CSi	CK	CCa	CTi	CMn	CFe2+
TUR2R1	1	15	88.21	0.46	1.13	3.78	3.66	0.00	0.05	0.05	0.00	0.50
TUR2R2	2	15	86.82	0.45	1.11	3.76	3.70	0.00	0.03	0.04	0.00	0.52
TUR3	3	15	85.83	0.54	1.04	3.68	3.69	0.00	0.00	0.07	0.00	0.66
BIO1	4	11	96.40	0.10	1.24	1.57	3.02	0.65	0.00	0.10	0.00	0.78
BIO2	5	11	92.19	0.06	1.31	1.53	2.85	0.74	0.00	0.17	0.00	0.96
FSP1	6	8	100.46	0.71	0.00	1.32	2.68	0.00	0.31	0.00	0.00	0.00
MUS1	7	11	97.21	0.09	0.01	1.44	4.03	1.24	0.00	0.00	0.00	0.05